K_o-BEHAVIOR OF NORMALLY CONSOLIDATED FINE-GRAINED SOILS DURING ONE-DIMENSIONAL SECONDARY COMPRESSION AGING AND THE QUANTITATIVE PREDICTION OF THE QUASI-PRECONSOLIDATION EFFECT

BY

RANDALL WAYNE BROWN

A DISSERTATION PRESENTED TO THE GRADUATE SCHOOL
OF THE UNIVERSITY OF FLORIDA IN
PARTIAL FULFILLMENT OF THE REQUIREMENTS
FOR THE DEGREE OF DOCTOR OF PHILOSOPHY

UNIVERSITY OF FLORIDA

1985

This dissertation is dedicated to the Lord Jesus Christ in grateful acknowledgment of His boundless blessings and His fulfilled promise:

> "Commit thy way unto the Lord; trust also in Him; and He shall bring it to pass." (Psalm 37:5)

This dissertation is also dedicated to my greatest blessings, Brenda and Matthew, in loving appreciation for their unselfish sacrifice, constant support, and endless love.

ACKNOWLEDGMENTS

As might be expected for an effort so broad in scope and time, the author has many people to recognize and thank. The author expresses his sincere appreciation to

1) The National Science Foundation for its sponsorship of the research;
2) The Air Force Engineering Services Center (AFESC) for additional fiscal support;
3) Colonel Robert Boyer and Dr. Paul Thompson of AFESC for arranging the support and providing needed encouragement;
4) Dr. John L. Davidson for his guidance and service as committee chairman and principal investigator;
5) Dr. John H. Schmertmann for his guidance and service as project consultant and co-principal investigator;
6) Dr. Frank C. Townsend for his instruction on laboratory techniques and equipment and his service on the supervisory committee;
7) Dr. James H. Schaub for providing additional funding for the research, service on the author's committee, and valuable direction in developing the format for this report;
8) Dr. Kermit L. Hall for his willingness to add committee service to a long list of commitments;

9) Professor William W. Coons for his valuable counsel and service on the committee;

10) Charles W. Manzione, the author's research partner and friend, for technical contributions, long hours, and encouragement;

11) James Pool, Shau Lei, and John Gill for their dedication as workers and friends;

12) Bill Studstill, Danny Richardson, Bill Whitehead, Karen Purser, Anita Hyde, and Pat Rossignol who each played a significant role in securing project logistics;

13) Dr. David Bloomquist for taking the time to teach the author about electronic and pressure systems;

14) Ms. Cindy Zimmerman and Ms. Lynne Parten for their assistance in preparing this manuscript;

15) Dr. George Boulton for his valuable advice and unwavering friendship throughout the author's graduate studies;

16) Each family member and friend who offered a word of encouragement and a prayer in the author's behalf.

Without the contributions of these people, this study would not have been completed.

TABLE OF CONTENTS

LIST OF TABLES

LIST OF FIGURES

Abstract of Dissertation Presented to the Graduate School
of the University of Florida in Partial Fulfillment of the
Requirements for the Degree of Doctor of Philosophy

K_o-BEHAVIOR OF NORMALLY CONSOLIDATED FINE-GRAINED SOILS DURING ONE-DIMENSIONAL SECONDARY COMPRESSION AGING AND THE QUANTITATIVE PREDICTION OF THE QUASI-PRECONSOLIDATION EFFECT

BY

RANDALL WAYNE BROWN

August 1985

Chairman: Dr. John L. Davidson
Major Department: Civil Engineering

No consensus and little experimental evidence exist in the geotechnical engineering community regarding K_o-behavior of normally consolidated fine-grained soils during one-dimensional secondary compression aging and the origin and magnitude of the quasi-preconsolidation effect.

After reviewing several concepts, a control volume triaxial-type test cell with support systems was developed. This equipment allows the maintenance and measurement of the K_o-condition during consolidation. Design considerations, development history, and performance parameters for the system are provided.

Six normally consolidated fine-grained specimens, three Edgar Plastic Kaolinite and three Agsco novaculite, were allowed to age a minimum of 14 days under a 2 tsf vertical stress while the

K_o-condition was maintained and measured. The specimens were loaded in small increments following aging to determine if the quasi-preconsolidation effect had developed.

Results show K_o decreases during secondary aging in one-dimensional compression for normally consolidated fine-grained soils. Moreover, the quasi-preconsolidation effect develops in both cohesive and cohesionless fine-grained soils. This suggests the quasi-preconsolidation effect develops due to increased friction rather than bonding as previously proposed. Finally, results indicate the existing theory for predicting the magnitude of the quasi-preconsolidation effect needs further refinement.

CHAPTER 1
INTRODUCTION

1.1 Problem Statement

Since the introduction of Karl Terzaghi's one-dimensional consolidation theory in 1923, geotechnical engineers have investigated phenomena which cause deviations from predictions based on his theory. In recent years, geotechnical researchers have offered the quasi-preconsolidation ($q\text{-}p_c$) phenomenon as an explanation for predicted settlements exceeding actual settlements in soils.

Although the existence of the $q\text{-}p_c$ effect is generally acknowledged, no such agreement exists regarding its origin. Currently, bond-increase and soil friction-increase phenomena contend for recognition as the cause of the $q\text{-}p_c$ effect. This lack of understanding regarding the $q\text{-}p_c$ effect has prevented its practical use in settlement calculations.

Over the past 40 months, the University of Florida (UF), under the direct sponsorship of the National Science Foundation (NSF) and ancillary sponsorship by the Air Force Engineering and Services Center (AFESC), studied the behavior of normally consolidated (NC) fine-grained soils during secondary compression aging, in general,

and the subsequent inferences regarding the $q\text{-}p_c$ effect, in particular. This paper discusses that study and its findings.

1.2 Purpose and Scope

The purpose of this study was to provide answers to the following questions:

1) For a normally consolidated fine-grained soil, does $K_o = \sigma'_3/\sigma'_1$ increase, decrease, or remain constant during secondary aging in one-dimensional compression?
2) Is the existing quantitative theory for predicting the $q\text{-}p_c$ effect (Schmertmann, 1981) accurate in light of the answer to question 1?

The research team established two specific objectives enroute to answering the questions above:

1) design and build a laboratory device to measure lateral soil pressures (and hence K_o) during one-dimensional consolidation, and
2) subject a variety of fine-grained soils to one-dimensional normal consolidation then to at least 14 days of secondary aging to determine changes in K_o with time.

Due to the disproportionate amount of time required to achieve the first objective, the research team focused on establishing a credible data base for two soils to present in this report.

1.3 Project History

As alluded to earlier, development of a K_o-consolidometer and execution of the accompanying test program was a time-consuming and expensive proposition. This section provides the prospective researcher an idea of potential problems and documents the contributions of the author's fellow UF researchers.

In March 1982, NSF provided Dr. John L. Davidson and Dr. John H. Schmertmann a grant (CEE-8116906) to study the behavior of NC fine-grained soils during secondary aging and to evaluate Dr. Schmertmann's quantitative theory for the $q\text{-}p_c$ effect. Under their direction and in consultation with Dr. Frank Townsend, W. David Stoutamire designed a K_o-consolidometer test cell and control system. Following Stoutamire's graduation in December 1982, graduate student Paul Sze began the first validation tests on the new equipment. During his tenure, the problem of temperature sensitivity was solved via construction of a styrofoam control room with thermostat. However, Sze's tests indicated unreasonably low K_o values and no explanation was found at that time.

At Sze's departure in December 1983, the author became the student investigator aided by master's student Michael Stefadouros. Stefadouros continued refinement of the K_o-consolidometer while the author prepared the IDS testing program, part of the original scope of the project. Stefadouros made progress in achieving reasonable K_o values by streamlining the system's design to eliminate excess and worn tubing where volume changes can occur. The Mark II control

board, built by Stefadouros in June 1984, reflected this simpler design. However, a new problem arose--a loss of water from the Volume Change Measurement Subsystem apparently unrelated to the consolidation process. In July 1984, the author and undergraduate assistant James Pool began a concerted effort to improve the equipment's performance and the project's productivity by building a mercury backpressure subsystem for each test cell and by continuing development of the Mark II testing equipment.

On August 16, 1984, the research team met at the author's request to review the progress, discuss the problems, and chart the course of the project. The research team decided to 1) request an extension to the project's deadline to allow more time for equipment development and testing, 2) abandon the IDS test phase of the project in light of dwindling time, money, and manpower resources, and 3) test only two soils due to these limited resources. Specifically, equipment development primarily dealt with the problems of low K_o values and the unexplained water loss.

Since August 16, 1984, the author and master's student Charles Manzione, aided by student assistant Shau Lei, further iterated the process of equipment refinement and soil testing. This final iteration included completion of the Mark II testing equipment, replacement of the Mark I control board, and a series of tests on two fine-grained soils. This report presents the results of the refinement/testing process, the dividend on an investment of approximately 60 man-months and $82,000 of combined NSF, AFESC, and UF funds.

CHAPTER 2
REVIEW OF THE LITERATURE

2.1 Introduction

The research team conducted two separate literature reviews during the project, each corresponding to a specific objective defined in Chapter 1. Stoutamire (1982) made an extensive survey of the laboratory techniques for determining K_o during one-dimensional consolidation before designing the UF K_o-consolidometer equipment. The author provides a synopsis of those findings in Chapter 4. The second literature review focused on previous and concurrent work on the $q\text{-}p_c$ effect. Specifically, this literature survey addressed three questions:

1) What is the $q\text{-}p_c$ effect and what theories have been offered to explain it?
2) What quantitative theories for predicting the $q\text{-}p_c$ effect exist and on what assumptions are these theories based?
3) What concurrent research is being done on the $q\text{-}p_c$ effect and the behavior of K_o during secondary compression aging?

This chapter reports the answers to these questions.

2.2 Qualitative Theories for the Quasi-Preconsolidation Effect

2.2.1 General

The q-p_c effect may be defined as the capability of an "aged" soil (a soil left under a constant effective stress over time) to carry "additional load without undergoing significant settlements" (Bjerrum, 1972, p. 18). Since the first observance of this phenomenon by Casagrande (1936), researchers have assumed the q-p_c effect existed only in cohesive soils and have predicated their qualitative theories for the q-p_c effect on this assumption. Qualitative theories based on this assumption all share the idea that temporary bonds are formed within the soil as the soil ages. However, no single explanation emerged as to how and why these bonds were formed. Schmertmann (1981) further stirred the controversy by suggesting the q-p_c effect was the result of frictional and not bonding behavior within the soil and thus the q-p_c effect also could exist in cohesionless soils. Schmertmann's theory likely will receive new interest and scrutiny upon publication of this study. The following section presents both bond and friction theories.

2.2.2 Qualitative Theories

Bond theories. Terzaghi (1941) postulated the first bond theory when he said highly viscous, adsorbed pore water was displaced over time and a rigid, solid bond gradually developed between clay particles. Tjong-Kie Tan (1957) also believed rigid bonds develop between mutually-connected plate-shape clay particles. Lambe (1960)

suggested cementation bonds develop over time as chemical weathering occurs in the presence of ferric oxides. Bjerrum and Wu (1960) also indicated chemical weathering may cause cementation bonds to develop over time. Bjerrum (1967) further noted that iron compounds created cementation between particles in Labrador quick clays exhibiting the $q\text{-}p_c$ effect. Moreover, Bjerrum purported the $q\text{-}p_c$ effect to be the result of increased bond strength as calcium Ca^{++}, magnesium Mg^{++}, aluminum Al^{+++}, ferrous Fe^{++}, ferric Fe^{+++}, or potassium K^{+} ions replaced sodium Na^{+} ions during chemical weathering.

To date, the most comprehensive examination of the $q\text{-}p_c$ effect in clays has been performed at Purdue University. Between 1955 and 1973, five separate studies were completed in an attempt to characterize and explain the $q\text{-}p_c$ effect. The Purdue theory, as reported by Leonards and Altschaeffl (1964) and reiterated by Davidson (1973, 1977), explains the formation of the $q\text{-}p_c$ effect as follows:

> during a period of time when a clay is subjected to constant applied stresses, water molecules become orientated in the vicinity of the edge-to-face contact points. Particles slowly displace or creep into "the most efficient arrangement possible from the standpoint of bond strength." . . . The mineral skeleton can now sustain pressure increments with very little deformation until sliding of particles is again initiated at the quasi-preconsolidation pressure. (Davidson, 1973, p. 26)

Friction theory. As noted earlier, Schmertmann's 1981 qualitative theory for the $q\text{-}p_c$ effect was a radical departure from the previous 40 years of attributing the effect to bonding. Schmertmann hypothesizes the following behavior:

> a clay can and will slowly readjust its fabric under drained conditions, such as during long periods of time at constant stress. The more easily dispersed (moved) particles . . . yield by particle-to-particle slippages to those . . . with more rigidity and which probably also have more strength and more resistance to dispersion. . . . With time the soil becomes stronger and stiffer as a result of the yield-transfer of applied shear to those stiffer and stronger aggregates. (Schmertmann, 1981, p. 477)

2.2.3 Summary

Until 1981, the $q\text{-}p_c$ effect was considered a phenomenon which only occurred in cohesive soils and resulted from stronger bonds being formed in the soil over time. No explanation as to how these bonds form has been universally accepted. In 1981, Schmertmann presented a new qualitative explanation of the $q\text{-}p_c$ effect. His theory attributes the $q\text{-}p_c$ effect to an increase of particle friction within the soil fabric and thus maintains the $q\text{-}p_c$ effect can exist in all soils. An examination of the test data on the cohesionless soil used in this study should dispel one of these theories.

2.3 Quantitative Prediction of the Quasi-Preconsolidation Effect

2.3.1 General

Apparently, the uncertainty which exists over the cause of the $q\text{-}p_c$ effect has precluded attempts to predict its magnitude. Indeed, Schmertmann (1981) is the only researcher to publish a quantitative theory for the $q\text{-}p_c$ effect. The following section discusses the

assumptions on which this theory was based and presents the formula for the $q\text{-}p_c$ effect.

2.3.2 Quantitative Theory

The underlying assumption to Schmertmann's quantitative theory is his soil friction-increase theory, as explained in Section 2.2.2. Specifically, Schmertmann assumed an effective stress path (ESP in Figure 2-1) based on this behavior and derived a formula to quantify the $q\text{-}p_c$ effect.

The ESP from point 0 to point 2 represents the phase where normal consolidation occurs. The ESP from point 2 to point 3 represents the aging phase where the soil friction-increase phenomenon is assumed to occur. The direction of the ESP from point 2 to point 3 is based on the assumption that K_o decreases during the aging phase. After this aging, the soil is subjected to vertical stress increases under the K_o-condition to test for the $q\text{-}p_c$ effect. This effect reaches its maximum when the ESP reaches point 4. "After reaching point 4, the additional volume and shear strains associated with further increasing effective stresses gradually destroy the special fabric dispersion effects that increased ϕ' [and decreased K_o] during the 2-3 aging, and the ESP eventually returns to the initial K_o-line at some point 5" (Schmertmann, 1981, p. 479).

From this stress path, Schmertmann derived the following expression for the $q\text{-}p_c$ effect:

$$\Delta p_{cq} = p_o \frac{2(1-A_q)(S_4-S_2)}{[1-(1-2A_q)S_4](1+S_2)}$$

where Δp_{cq} = the magnitude of the q-p_c effect;

$p_o = \sigma_1'$ = the normal consolidation pressure;

S_2 = the slope of the initial K_o-line;

S_4 = the slope of the K_o-line after the q-p_c effect; and,

A_q = the net effect of the pore pressure parameter A over the entire 2-4 ESP of the q-p_c process.

2.3.3 Summary

Schmertmann (1981) has published the only theory to predict the magnitude of the q-p_c effect. Schmertmann assumed a stress path based on his qualitative soil friction-increase theory and derived a formula to express the q-p_c effect. Data from this research will be important in evaluating his assumptions and theory.

2.4 Concurrent Research on the Quasi-Preconsolidation Effect and K_o-Behavior During Secondary Compression Aging

2.4.1 General

During the past 40 months, the research team strove to keep abreast of concurrent research on the q-p_c effect and K_o-behavior during secondary compression aging. This effort was expedited by the publication of Schmertmann's technical note which posed the question: "Will $K_o = \sigma_3'/\sigma_1'$ of a normally consolidated cohesive soil increase or decrease during secondary aging in one-dimensional compression?" (Schmertmann, 1983, p. 121).

In this note, Schmertmann explained he had assumed K_o decreased while developing his quantitative theory for the q-p_c effect for his

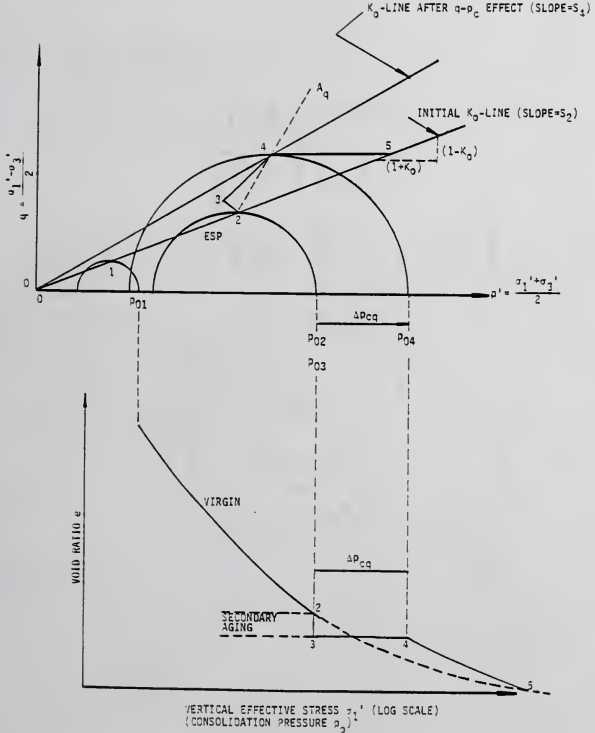

Figure 2-1 Effective Stress Path (ESP) before, during, and after the q-p_c effect (Modified after Schmertmann, 1981, p. 479)

1981 paper and that a "prominent reviewer" challenged this assumption. This challenge prompted Schmertmann to poll 40 geotechnical engineers, renowned for their work in soil consolidation, for their opinions. As reported in the technical note, his survey indicated there was no consensus of opinion regarding K_o-behavior during secondary aging.

Responses published subsequent to Schmertmann's technical note revealed a broad interest and several research efforts toward answering the K_o-behavior question. However, these research efforts did not address the application of this answer to the development of qualitative and quantitative theories for the q-p_c effect. Section 2.4.2 offers the information presently available on concurrent research efforts.

2.4.2 Concurrent Research

Kavazanjian and Mitchell (1984) concluded that K_o would increase for NC saturated clays and decrease for OC saturated clays. This suggestion was based on "limited, though fairly conclusive" triaxial cell data for two clays (undisturbed San Francisco Bay Mud and compacted kaolinite) and on a theoretical analysis using the Singh-Mitchell three-parameter creep equation. In a June 1984 telephone conversation with the author, Dr. Kavazanjian said he was seeking to expand his data base by further K_o-tests using a modified triaxial apparatus (Borja, 1984; Hsieh, 1984) and would welcome "further exchange on this topic." To date, representative soil samples have

been exchanged between the Stanford and UF research teams but no comparative tests have been completed.

Soydemir (1984) also concluded K_o increases with aging for NC cohesive soils. Soydemir based his answer on a mathematical analysis of two viscoelastic models, the Kelvin and the Maxwell. Of importance to note, Soydemir's answer is based on an assumption of viscoelasticity and no experimental evidence.

McRoberts (1984) argues that "K_o will remain the same with aging because secondary compression occurs because of a gradual transition from macropore to micropore dominated drainage" (Schmertmann, 1984, p. 673). Again, McRoberts' argument is no more concrete than Soydemir's because he assumes a behavior and offers no direct experimental evidence to support his assumption.

Nagaraj (1984) and Allam and Sridharan (1984) agree with Schmertmann's contention that K_o will decrease during aging. Moreover, they agree with Schmertmann's assumption that "changes in clay structure during aging that produce an increase in clay modulus and strength . . . would produce a decrease in K_o when strain rate continues to decrease during the aging" (Schmertmann, 1984, p. 673).

Discussions appearing in foreign geotechnical journals depicted the same confusion over the answer to Schmertmann's question as in American journals. For example, Japanese researchers Hanzawa (1983) and Yasuhara (1983) offered experimental data suggesting the constancy of K_o with aging. However, Yasuhara (1984) presents experimental evidence to suggest K_o decreases with aging. Yasuhara and Ue (1984) emphasize the variation of K_o during one-dimensional

consolidation is very sensitive to methods and devices used to measure it.

In the latest discussion of the K_o-behavior question, Jamiolkowski et al. (1985) cited test results on undisturbed Panigaglia clay using a square oedometer with a flush pressure transducer at Studio Geotechnico Italiano of Milan and on two organic silty clays using the MIT Lateral Stress Oedometer as evidence that K_o is constant during secondary compression aging. Moreover, those researchers say Kavazanjian and Mitchell's views "either do not apply to all cohesive soils or are premature" (Jamiolkowski et al., 1985, p. 33).

2.4.3 Summary

The UF research team, aided by published responses to Schmertmann's 1983 technical note, gathered information regarding concurrent research efforts on the $q\text{-}p_c$ effect and K_o-behavior during secondary compression aging. From this effort, the UF researchers learned

1) many opinions, though most unsubstantiated with experimental evidence, exist regarding K_o-behavior during aging;
2) current research efforts, excluding the UF effort, do not address the application of K_o-behavior to the development of qualitative and quantitative theories for the $q\text{-}p_c$ effect; and

3) results of K_o-behavior studies seem very sensitive to the methods and equipment employed.

In other words, the questions which prompted this study (reference Section 1.2) were not answered in concurrent research efforts.

CHAPTER 3
MATERIALS

3.1 Introduction

The three criteria for selecting the soils to be tested were

1) Was a large quantity of the material readily available for the preparation of duplicate specimens as dictated by the extended and iterative nature of the project?
2) Was some previous information on the soil's behavior available as a guide for separating equipment and procedural deficiencies from actual soil behavior during the developmental phase?
3) Was the soil either a cohesive, fine-grained or a cohesionless, fine-grained material as required by the scope of the study?

The cohesive, fine-grained material or clay selected was kaolinite from the Feldspar Corporation-EPK Clay Division in Edgar, Florida. The cohesionless, fine-grained material or silt selected was novaculite from the Agsco Corporation in Wheeling, Illinois. The following sections discuss the general properties and preparation procedures for each of these materials.

3.2 Edgar Plastic Kaolinite

3.2.1 General Properties

Edgar Plastic Kaolinite was a particularly attractive choice since it was available in large quantities at no cost due to the generosity of Hugh Cannon, general manager of the EPK Division of Feldspar Corporation. Moreover, this material had been used frequently in instruction and research at the University of Florida, including some of Dr. Schmertmann's earlier work. Hence, several sources could be tapped regarding its general properties and preparation.

From a combination of supplier's data, laboratory data, and historical data, the properties of Edgar Plastic Kaolinite may be listed as

Specific gravity of solids, $G_s = 2.59$

Liquid Limit, LL = 54.2%

Plastic Limit, PL = 29.2%

Plasticity Index, PI = LL-PL = 25.0%

Particles less than 2μ = 58.5%

Activity, PI/Particles less than 2μ = 0.43

Unified Soil Classification = CH

3.2.2 Specimen Preparation

This section presents an overview of Edgar Plastic Kaolinite preparation procedures. A detailed account, complete with

step-by-step instructions and photographs, is presented in a companion report by Manzione (1985).

Edgar Plastic Kaolinite is received in dry, powdered form. This powder is mixed with distilled water to a predetermined water content of 40% and then cured overnight. Next, the mixture is circulated through a Vac-Aire ceramic extruder (Figure 3-1) while under vacuum to achieve thorough mixing and de-airing. At the end of the fourth pass through the extruder, the specimen is cut, rolled in waxed paper, and dipped in warm wax three times to prevent moisture loss by evaporation. The UF research team also found wrapping the specimen in cellophane after waxing an effective deterrent to evaporation. The specimens, designated EPKW, are stored in a steel cabinet in the temperature control room until needed. Immediately prior to the start of a test, the cellophane and waxed paper are carefully removed and the specimen is placed in the cutting ring and trimmed to the proper size using a wire saw (Figure 3-2). The trimmed specimen is weighed and measured and water content determinations made from the cuttings. The specimen is now prepared for insertion into the test cell.

The Vac-Aire ceramic extruder allowed the research team to produce a large number of specimens with a high degree of saturation and similar structure throughout the project. The average degree of saturation for the extruded specimens used in Tests A, B, and C was 92.1%.

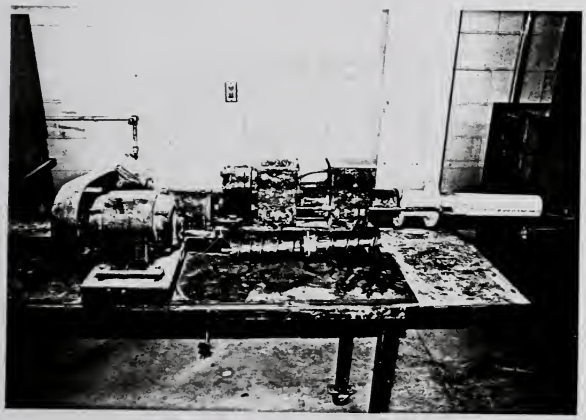

Figure 3-1 Vac-Aire Ceramic Extruder

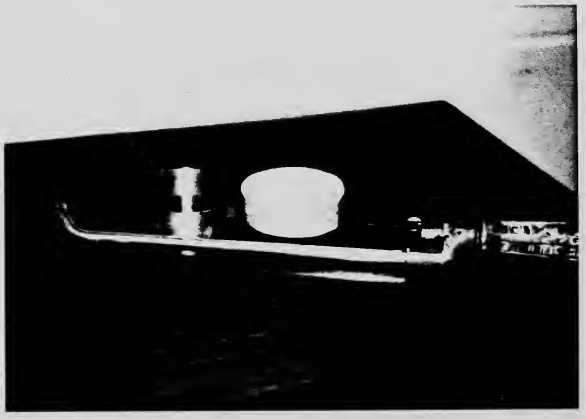

Figure 3-2 Cutting Ring, Wire Saw, and Trimmed EPKW Specimen

3.3 Novaculite

3.3.1 General Properties

Novaculite is not a soil in the traditional sense of the word. Rather, novaculite is an industrial abrasive created by grinding very hard, dense, even-textured, silica-bearing rock into fine particles. Novaculite is used in the manufacturing of glass and whetstones. One hundred pounds of novaculite were purchased from Agsco Corporation for use as the cohesionless, fine-grained material in this research. Although some work with novaculite was done at UF in the late 1950's and early 1960's, little was published and laboratory notes from that era were sketchy. Consequently, the bulk of information on novaculite and its preparation was found through the manufacturer and experimentation.

The properties of Agsco novaculite include

Specific gravity of solids, G_s = 2.65

Plasticity Index, PI = 0 (nonplastic)

Particles less than #200 sieve (74u) = 98.12%

Unified Soil Classification = ML

Hardness = Moh's Scale 7

3.3.2 Specimen Preparation

This section summarizes the procedures for preparing novaculite specimens. Again, Manzione (1985) addresses the intracacies of "how to" in his report.

Novaculite is also received in dry, powdered form. Fellow researchers should use extreme caution when handling this material in powdered form because exposure can result in silicosis and eye irritation. Thus protected by dust masks and goggles, researchers mix the powder with distilled water to a predetermined water content of 33.58%. This water content is significant because the material is easily handled as a paste which can be spooned into a specimen mold. Water contents above or below this point make the material difficult to handle. The paste is spooned into the mold in three lifts with the mold moved across a glass plate 10 times after each lift. The material is allowed to cure overnight in the mold. Immediately before the test, the mold is gently removed and the specimen is weighed and measured before insertion into the test cell (Figure 3-3). Curing drops the water content to 20.97% and creates a solid specimen with which to work.

The procedures described above were developed to fill the knowledge void regarding novaculite specimens. This development included a misguided attempt at producing novaculite specimens using the ceramic extruder. Despite this minor setback, the final procedures successfully produced a large quantity of uniform specimens, designated NOVW. The cured specimens had an average degree of saturation of 69.5% at insertion. Complete saturation of the NOVW specimens was easily achieved at low backpressures as discussed in Section 4.4.

Figure 3-3 NOVW Specimen and Mold

CHAPTER 4
EQUIPMENT AND PROCEDURES

4.1 Introduction

This chapter examines the design and operation of the UF K_o-consolidometer. Section 4.2 summarizes the initial design process. Section 4.3 reviews the individual subsystems which comprise the final system design. Section 4.4 synopsizes the soil testing procedures. Chapter 4 is not intended to be a handbook for the construction and operation of a K_o-consolidometer. Such details are available in the aforementioned companion report by Manzione (1985). Rather, this chapter explains the evolution of the UF K_o-consolidometer design and soil test procedures.

4.2 System Concept Selection

As previously noted in Section 1.3, the research team spent the majority of 1982 developing an initial design for the UF K_o-consolidometer. Stoutamire (1982) excellently recounts this initial design process. This process involved four steps: 1) defining the required basic functions of the system, 2) converting the functions into design parameters and performance specifications, 3) generating a list of alternatives to fulfill the parameters and specifications,

and 4) developing a workable design of the alternative selected in Step 3.

In Step 1, the research team identified the basic functions as 1) prevent strain, 2) apply stress, 3) measure stress, 4) drain water, 5) maintain stress, and 6) minimize friction.

Step 2 required translating these functions into design parameters and performance specifications. Table 4-1 lists each function with its associated desiderata.

In Step 3, Stoutamire generated a list of alternatives to satisfy the design requirements based on his review of technical literature, manufacturer's catalogs, and references on fabrication materials. In consultation with the remainder of the research team, Stoutamire subjectively rated each alternative according to its ability to meet the functional requirements. Each system received a score from 1 to 5, the larger value representing a better ability to satisfy the functional requirement. Table 4-2 presents the results of the evaluation.

Step 4 involved generating a detailed design for the selected controlled-volume triaxial cell concept. Specifics of the current UF K_o-consolidometer system are provided in Section 4.3 and Manzione (1985). However, an overview of how the system functions as a whole seems appropriate before examining the individual subsystems.

After the specimen is placed in the test cell, the specimen is backpressured to achieve saturation. When the specimen and system are fully saturated, vertical stress is applied incrementally to the specimen. Each vertical stress increment causes the specimen to try

Table 4-1 Basic Functions, Design Parameters, and Performance Specifications for the UF K_o-Consolidometer

Basic Function	Design Parameters and Performance Specifications
Prevent Strain	$10*10^{-6}$ in/in lateral strain tolerance
Apply Stress	0-111 psi variable lateral stress capability
Measure Stress	±0.1 psi lateral stress sensitivity ±0.1 psi pore pressure sensitivity 222 psi pore pressure capacity
Drain Water	Drainage without disturbance to the specimen or other functions
Maintain Stress	±0.1 psi stress tolerance over 30 days
Reduce Friction	Reduce or eliminate skin friction on the specimen without interference with other functions

Table 4-2 Functional Analysis of Alternative K_o-Consolidometers

System	Function					Total
	Prevent Strain	Apply Stress	Measure Stress	Maintain Stress	Minimize Friction	
1. Semirigid Confining Ring	1	3	2	1	3	10
2. Null Confining Ring	5	3	4	2	2	16
3. Null Triaxial	3	3	3	2	4	15
4. Control Volume Triaxial	5	3	5	4	4	21
5. Rigid Cell	5	3	5	4	3	20
6. University of Washington Stress Meter	1	3	3	4	2	13
7. Slurry Consolidometer	1	3	1	4	1	10

Source: Stoutamire, 1982, p. 74.

to strain laterally (bulge) as indicated on the mercury manometer. Lateral stress is applied until the manometer indicates the specimen is neither bulging nor compressing laterally, the K_o-condition. Following application of the last vertical stress increment and the ensuing dissipation of pore pressures, the lateral stress is regulated at frequent intervals to keep the specimen at the K_o-condition for at least 14 days. The lateral stress required and pore pressure measurements are recorded at every interval.

Three versions of the UF K_o-consolidometer system were built during the project. The original system, Mark I, was dismantled for parts in December 1984 after a history of inadequate performance. The Mark II system, which began operations in September 1984, performed well and featured a simpler, streamlined construction. Salvaging some Mark I parts, the Mark III system was built after the Mark II design to double soil testing capability. Mark III has also performed well. Figure 4-1 offers a schematic of the Mark II/Mark III systems. Figures 4-2 and 4-3 show the Mark II and Mark III control boards, respectively. Section 4.3 reviews the construction, function, and performance capability of the subsystems which comprise the UF K_o-consolidometer Mark II/Mark III systems.

4.3 Individual Subsystems

4.3.1 The Test Cell

The test cell was constructed to achieve the six basic functions at the least cost. The cell (Figure 4-4) was machined from stock

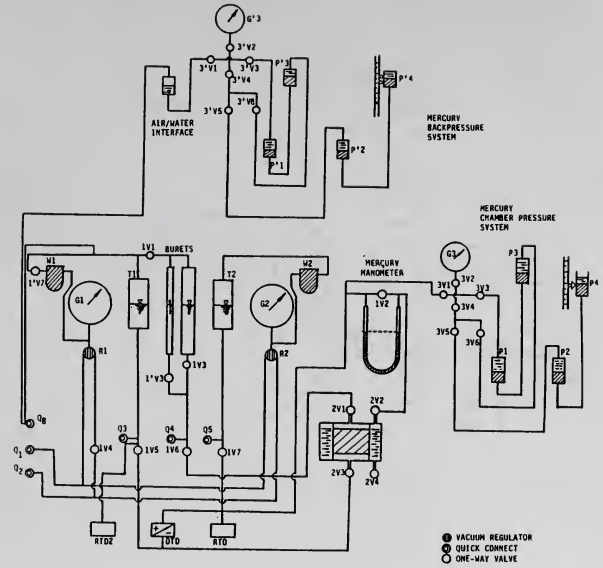

Figure 4-1 Schematic of UF K_o-Consolidometer Mark II/Mark III Systems

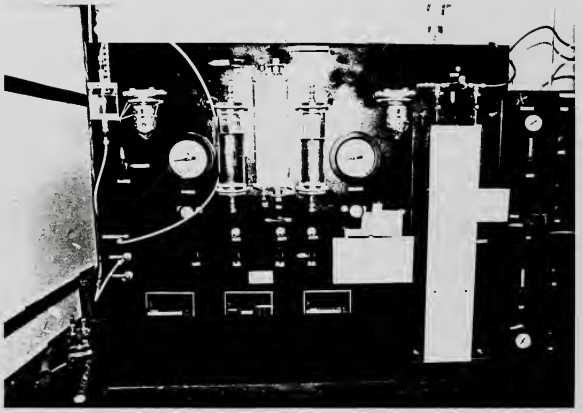

Figure 4-2 UF K_o-Consolidometer Mark II Control Board

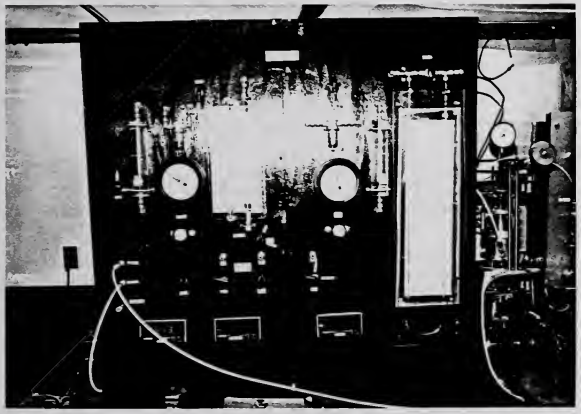

Figure 4-3 UF K_o-Consolidometer Mark III Control Board

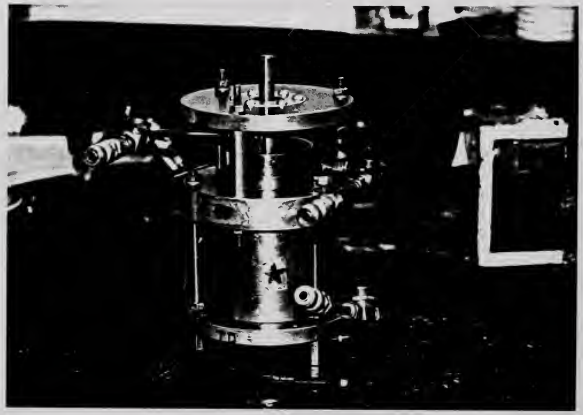

Figure 4-4 The UF K_o-Consolidometer Test Cell

aluminum plate and pipe. Cell joints are sealed with standard stock O-rings and brass tube fittings allow sample drainage and pressure application. The 3.00 inch-diameter piston was machined from stainless steel. Vertical load is transmitted to the piston via a 0.5 inch-diameter steel rod press fitted into the piston. The steel rod rides in two Thomson stainless steel linear ball bushings. The cell is constructed to handle a soil specimen 3.00 inches in diameter and 0.75 inches high placed between two stainless steel porous discs and surrounded by a rubber membrane (Figure 4-5).

Table 4-3 explains how the construction features cited above relate to fulfilling the basic functions of the system.

4.3.2 Backpressure/De-airing Subsystem (BPDS)

The major components of the BPDS (Figure 4-1) are the pressure source, the air/water interface tank T1, and a Sensotec Model TJE/708 pressure transducer wired to a Doric Model 420 Transducer Indicator (RTD2 in Figure 4-1). The Sensotec Model TJE/708 pressure transducer has a capacity of 150 psi. These components are connected to each other and to the test cell via .25 inch-outside diameter Nylaflow pressure tubing. The pressure source employed varies according to need. The specimen is brought to the desired backpressure using regulator R1 from the air compressor then switched to the mercury backpressure system which provides a more stable backpressure over long periods of time.

The functions of the BPDS are 1) dissolve pockets of air in the specimen and system to achieve a saturated specimen before loading

Figure 4-5 Interior of Test Cell Showing Specimen and Porous Discs Sealed in Rubber Membrane

Table 4-3 Correlation of Basic Functions to Test Cell Construction Features

Function	Construction Feature
Prevent Strain	Displacement of water in cell chamber changes mercury manometer level indicating lateral stress needs to be adjusted to prevent lateral strain.
Apply Stress	1) Line 2V2 (Figure 4-1) allows lateral pressure to be decreased or increased in the chamber to maintain the K_o-condition. 2) Vertical stress is transmitted via the stainless steel piston from the 0.5 inch-diameter rod in contact with the oedometer loading frame.
Measure Stress	Line 2V2 (Figure 4-1) is connected to the pressure transducer RTD for the measurement of lateral stress.
Drain Water	Water drains through the top stainless steel disc and the top platten into Line 2V1 (Figure 4-1) displacing water in the small buret.
Maintain Stress	1) Line 2V2 (Figure 4-1) is connected to an adjustable mercury pot system, noted as a steady pressure source. 2) The piston transmits a dead load placed on an oedometer loading frame; the dead load is constant.
Reduce Friction	1) A rubber membrane is used to surround the specimen to preclude side friction and shear stresses. 2) The 0.5 inch-diameter rod rides in two Thomson stainless teel linear ball bushings to minimize friction and load eccentricity. 3) The piston is polished to a mirror finish and coated lightly with a mixture of silicon and glycerine to minimize friction.

begins and 2) provide a constant backpressure after loading begins. Each of these functions relates to the system's ability to measure stress and maintain stress.

The backpressure may be adjusted to any pressure desired by adjusting regulator R1 or by turning the winch (Figure 4-6) to adjust the height of the mercury pot, depending on the pressure source in use. The maximum backpressure available is 100 psi using regulator R1 and 111 psi using the mercury backpressure system. A tandem pot arrangement (Figure 4-1) was necessary to achieve the 111 psi capability on the mercury backpressure system. The Doric allows the backpressure to be read to the nearest .01 psi, as measured by the Sensotec pressure transducer.

4.3.3 Vertical Stress Application Subsystem (VSAS)

The VSAS consists of a modified Soiltest Model C-221 oedometer and a Soiltest Model LC-3 dial gage (Figure 4-7). The oedometer is modified to accommodate the 8-inch high test cell by replacing the standard 3 inch threaded rods with 16 inch rods. The dial gage is attached to the top frame to measure vertical deflections.

The functions of the VSAS are 1) apply vertical stress and 2) measure vertical deformation.

The oedometer has a load capacity of 16 tons per square foot or 220 psi. Vertical deflections can be read on the dial gage to the nearest .0001 inch and estimated to the nearest .00001 inch.

Figure 4-6 Winch for Adjusting Backpressure/De-airing Subsystem (BPDS)

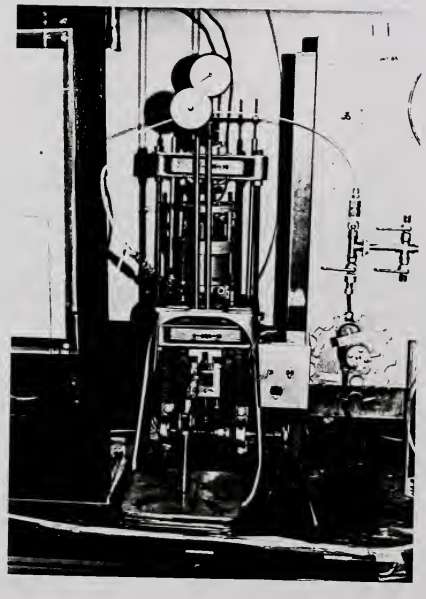

Figure 4-7 Vertical Stress Application Subsystem (VSAS)

4.3.4 Lateral Strain Null Subsystem (LSNS)

The LSNS is simply a "U" column partially filled with mercury, sometimes referred to as a mercury manometer (Figure 4-8). One branch of the "U" is connected to the test cell's top chamber outlet via .25 inch-outside diameter copper tubing and the other to the Lateral Stress Application Subsystem (LSAS) as shown in Figure 4-1.

The LSNS helps the system prevent strain, apply stress, and measure stress. By observing the mercury level in the "U," the researcher can detect movement of cell water caused by lateral straining of the soil. Specifically, if the mercury level in the right side of the "U" is above the pretest level, the lateral pressure being applied exceeds that necessary for the K_o-condition. Conversely, if the level is below, more pressure is needed for the K_o-condition. The researcher uses the LSNS as a guide for applying stress and as an indicator that true K_o-values may be computed from measured stresses.

The LSNS scale may be read to the nearest .01 inch. The diameter of the mercury manometer is .0197 in (.5 mm). Thus, the manometer can detect volumetric strains as small as $\pm .6*10^{-6}$ in^3/in^3 and lateral strains as small as $\pm 6*10^{-6}$ in/in, using .75 and 3 inches as the specimen height and diameter, respectively.

4.3.5 Lateral Stress Application Subsystem (LSAS)

The major components of the LSAS are the pressure source and a Sensotec Model TJE/708 pressure transducer wired to a Doric Model 420 Transducer Indicator (RTD in Figure 4-1). Recall, the Sensotec Model

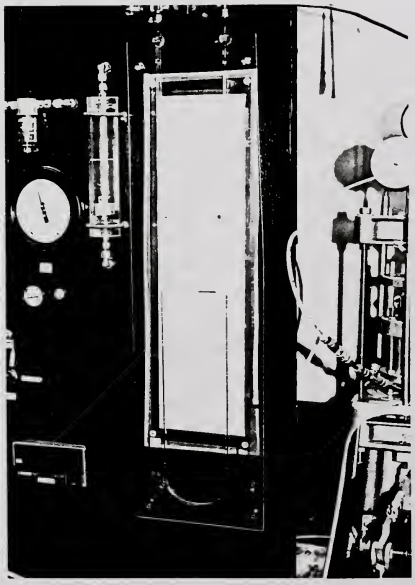

Figure 4-8 Lateral Strain Null Subsystem (LSNS)

TJE/708 pressure transducer has a capacity of 150 psi. During the first hour of each load increment, the lateral pressure is adjusted using regulator R2 since frequent and rapid adjustments are required (Figure 4-1). At other times, the mercury pot system serves as the source of lateral pressure because of its ability to maintain pressure with little fluctuation over long periods of time (Figure 4-1). Both pressure sources are connected to the LSNS, and hence to the test cell, with .25 inch-outside diameter Nylaflow pressure tubing.

The LSAS fulfills the basic functions of applying, maintaining, and measuring stress.

The lateral stress may be adjusted to any pressure necessary by adjusting Regulator R2 or by turning the winch (Figure 4-9) to adjust the height of the mercury pot, depending on the pressure source in use. The maximum lateral pressure available is 100 psi using regulator R2 and 111 psi using the mercury pot system. The Doric allows the lateral pressure to be read to the nearest .01 psi, as measured by the Sensotec pressure transducer.

4.3.6 Pore Pressure Measurement Subsystem (PPMS)

The major component of the PPMS is a Sensotec Model TJE/741 differential pressure transducer wired to a Doric Model 420 Transducer Indicator (DTD in Figure 4-1). The Sensotec Model TJE/741 differential pressure transducer has a capacity of 50 psi. This transducer measures the pressure difference between the pore water pressure at the bottom of the specimen and the applied lateral

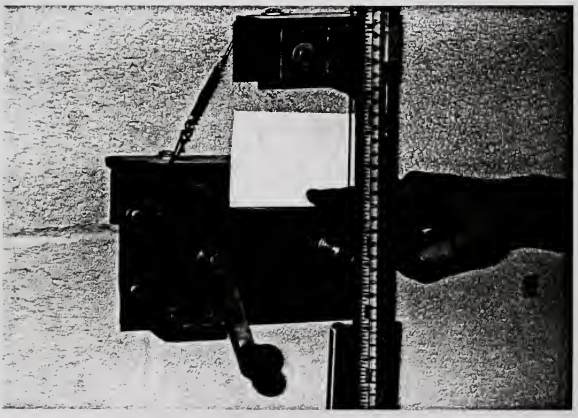

Figure 4-9 Winch for Adjusting Lateral Stress Application Subsystem (LSAS)

stress. Subtracting the DTD value and the RTD2 values from RTD yields the excess pore pressure. The differential transducer is connected to the bottom of the specimen with .25 inch-outside diameter Nylaflow tubing and to the LSNS with a combination of .25 inch-outside diameter Nylaflow and copper tubing.

Figure 4-10 shows all three transducers used in the UF K_o-consolidometer system. The differential transducer is the large body in the center of the photograph. All three transducers are mounted at an elevation coincident with the specimen's centerline to eliminate the need for elevation corrections.

The PPMS contributes to the "measure stress" function of the system.

The Doric allows the differential pressure to be read to the nearest .01 psi, as measured by the differential transducer.

4.3.7 Volume Change Measurement Subsystem (VCMS)

The VCMS consists of a small bore buret connected to the top specimen drainage port of the test cell via a combination of .25 inch-outside diameter copper and Nylaflow tubing (Figure 4-1). The cross-sectional area of the burets are .018 in^2 and .016 in^2 for the Mark II and Mark III systems, respectively. Figure 4-11 shows a close-up of the small buret with the large overflow buret. The Mark II VCMS employs 6 ft of copper and 5 ft of Nylaflow tubing. The Mark III VCMS has approximately 4.5 ft of copper and 3.5 ft of Nylaflow tubing. Copper tubing was installed where possible due to Nylaflow's

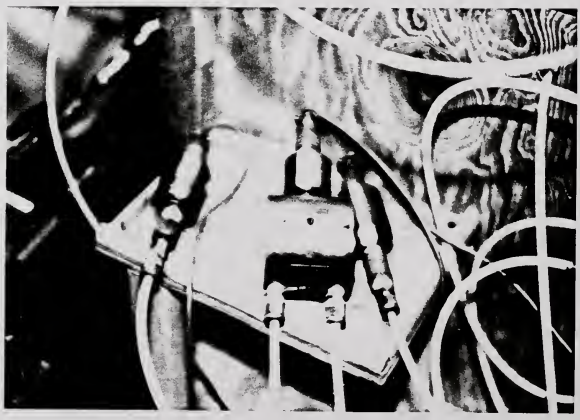

Figure 4-10 Pore Pressure Measurement Subsystem (PPMS) Components: Sensotec Model TJE/741 Differential Pressure Transducer (Center) and Sensotec Model TJE/708 Pressure Transducers (Left and Right)

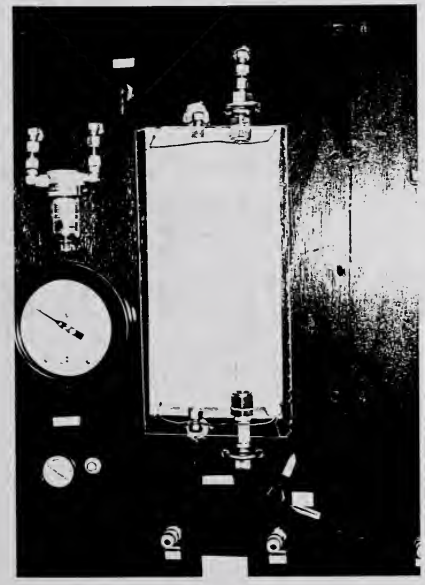

Figure 4-11 Volume Change Measurement Subsystem (VCMS)

absorption/evaporation characteristics, a topic which will be discussed in detail later in this report.

The function of the VCMS is to drain water. In addition, the VCMS provides a check on the LSNS since the water expelled from the specimen should equal the vertical change in specimen height times the specimen area for the K_o-condition.

The divisions on the VCMS are .05 inches and may be estimated to the nearest .01 inch. Therefore, the change in volume may be calculated to the nearest .00018 in^3 and .00016 in^3 for the Mark II and Mark III systems, respectively.

4.3.8 Temperature Control Subsystem (TCS)

The three components of the TCS are the temperature control room, an Omega thermostat, and an Arvin portable electric heater. The temperature control room (Figure 4-12) is constructed of .5 inch-thick styrofoam panels sealed with polyethylene and duct tape. Plexiglass windows allow cursory equipment checks and light from outside the room. The Omega thermostat may be set for any temperature between 75°F and 125°F (Figure 4-13). When the temperature drops below that desired, the thermostat turns on the electric heater (Figure 4-14) to raise the room temperature. Fortunately, temperatures were not prone to rise above the desired level; therefore no cooling element was provided for the TCS.

The function of the TCS is to maintain a constant temperature. A constant temperature is necessary so the system can achieve its six basic functions. Specifically, temperature variations will cause the

Figure 4-12 Temperature Control Subsystem (TCS)--Temperature Control Room

Figure 4-13 Temperature Control Subsystem(TCS)--Omega Thermostat

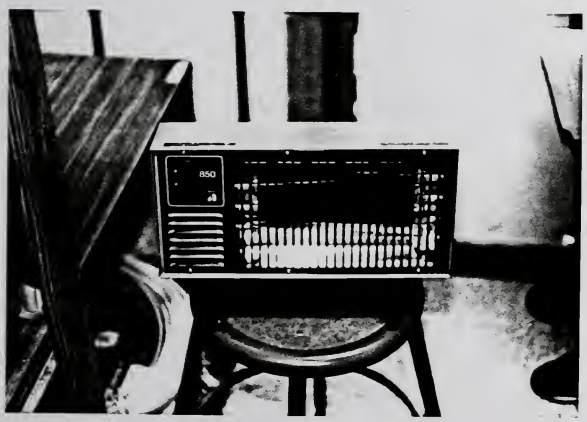

Figure 4-14 Temperature Control Subsystem (TCS)--Arvin Portable Electric Heater

chamber, tubing, and water to expand or contract. Moreover, sealed systems act as thermometers. Hence, all tests were conducted in the temperature control room.

The divisions on the Omega thermostat are 1°F and may be estimated to the nearest .1°F.

4.4 Soil Testing Procedures

This section presents a synopsis of how to test a soil in the UF K_o-consolidometer. Again, Manzione (1985) should be consulted for step-by-step details. The test is conducted in these five phases:

1) Prepare the specimen. This entails trimming, measuring, and weighing the specimen before placement in the test cell.
2) Backpressure the specimen. The specimen is placed under a constant backpressure to dissolve air pockets in the specimen and system so full saturation can be achieved. Backpressure typically takes 3 days and 1 day for kaolinite and novaculite, respectively. B-value checks are conducted to insure the specimen is fully saturated before proceeding with the next step.
3) Load the specimen. Vertical stress is applied in three increments of .5, 1, and 2 tsf. The K_o-condition is maintained by adjusting the lateral stress as indicated by the mercury manometer (LSNS). The excess pore pressure is allowed to dissipate following each load increment before the

next increment is applied. Dissipation typically takes 18-24 hours for kaolinite and .5-4 hours for novaculite.

4) Age the specimen. The specimen is allowed to sit under the constant vertical stress of 2 tsf for a minimum of 14 days. During this time, the lateral stress is adjusted to maintain the K_o-condition as indicated by the mercury manometer (LSNS). Deformation, stress, drainage, and temperature of the specimen are monitored at frequent intervals, usually every 2-4 hours.

5) Load the specimen. Finally, the K_o-condition is maintained while the specimen is loaded in small increments to determine the magnitude of the q-p_c effect.

Although broad in scope, the previous discussion should aid in understanding the data and analysis to follow.

CHAPTER 5
COMPUTATIONS AND RESULTS

5.1 Introduction

This chapter reviews the data gathering/reduction process and presents the test results. Section 5.2 discusses the observed data. Section 5.3 explains how new information was developed by reducing the observed data. Finally, Section 5.4 offers the test results.

The data and results presented in this chapter are for six K_o-consolidation tests conducted between September 28, 1984, and April 19, 1985. As prescribed by the principal investigators, each test presented herein is a "perfect" test. A "perfect" test is defined as a test free from any known equipment or procedural deficiencies. The remainder of time in the final testing phase, the period cited above, was spent developing the final design and procedures discussed earlier so "perfect" tests could be achieved.

5.2 Observed Data

5.2.1 Before Test

Before each test, the specimen was trimmed, measured, and weighed. Specimen trimmings were weighed, oven dried, and weighed

again to determine the water content of the specimen. The diameter and height were each measured 3 times to the nearest .001 cm using a Mitutoyo micrometer. The specimen was weighed to the nearest .01 g using a Mettler balance. The specific gravity of solids was known for both materials.

5.2.2 During Test

Throughout the K_o-consolidation test, 10 pieces of information are noted. The data are date, time, chamber pressure, differential pressure, backpressure, small buret level, large buret level, manometer level, dial gage reading, and temperature. The degree of accuracy for these measurements was discussed in Chapter 4.

5.3 Reduced Data

5.3.1 Before Test

Using the observed data, the volume, volume of solids, height of solids, initial void ratio, area, and total unit weight may be computed as shown in Figure 5-1.

5.3.2 During Test

Knowing the data observed before and during the test and the reduced pretest data, values may be determined for excess pore pressure, average pore pressure, lateral effective stress, vertical effective stress, K_o, p', q', change in specimen height, and void ratio. After calculating the values for K_o and void ratio,

SYMBOLS:

w = water content
W = weight of specimen
d = diameter of specimen
H = initial height of specimen
G_s = specific gravity of solids
A = area of specimen
V = volume of specimen
W_s = weight of solids
V_s = volume of solids
H_s = height of solids
e_o = initial void ratio
γ = total unit weight
γ_w = unit weight of water

OBSERVED: w, W, d, H, G_s

COMPUTED:

$A = \frac{1}{4}\pi d^2$
$V = AH$
$W_s = W/(1+w)$
$V_s = (W_s/G_s)\gamma_w$
$H_s = V_s/A$
$e_o = (V-V_s)/V_s$
$\gamma = W/V$

Figure 5-1 Chart for Reduction of "Before Test" Data

correlations such as aged K_o values as a percentage of the pre-aging K_o value and void ratio as a percentage of initial void ratio may be found. Figure 5-2 shows the data reduction sequence.

5.4 Test Results

This section presents the specimen data and test results for the six K_o-consolidation tests run using the equipment and procedures previously discussed. Table 5-1 provides information regarding the testing schedule. Table 5-2 characterizes the specimens tested. Figures 5-3 and 5-4 examine the behavior of K_o with aging time for EPKW and NOVW specimens, respectively. Figures 5-5 through 5-10 are p'-q diagrams for the six tests marked with Schmertmann's quantitative theory notation (see Figure 2-1). Figures 5-11 through 5-16 are e-log σ_1' plots reflecting the graphical solution for the q-p_c effect. Appendices A through F include tables and raw plots for Tests A through F, respectively. Tables 5-3 and 5-4 summarize the information presented in this section and Appendices A through F. Appendix H presents sample calculations showing step-by-step computation of the information in Table 5-4. These tables should provide the reader an easy reference for the discussion of results in Chapter 6.

SYMBOLS:

- H = initial height of specimen
- H_s = height of solids
- e_o = initial void ratio
- σ_3 = chamber pressure
- DTD = differential pressure between the chamber and the pore pressure at the bottom of the specimen
- BP = backpressure
- DR = dial reading
- σ_1 = vertical stress
- u = average pore pressure
- σ_1' = vertical effective stress
- σ_3' = lateral effective stress
- K_o = lateral stress ratio for one-dimensional strain
- ΔH = change in height
- e = void ratio

KNOWN: H_s, e_o, σ_1

OBSERVED: σ_3, DTD, BP, DR

COMPUTED:

$$\text{EXCESS PWP} = \sigma_3 - \text{DTD} - \text{BP}$$

$$u = \frac{2}{3}(\text{EXCESS PWP}) + \text{BP}$$

$$\sigma_1' = \sigma_1 - u$$

$$\sigma_3' = \sigma_3 - u$$

$$K_o = \sigma_3'/\sigma_1'$$

$$p' = (\sigma_1' + \sigma_3')/2$$

$$q = (\sigma_1' - \sigma_3')/2$$

$$\Delta H = H - \Delta DR$$

$$e = e_o - (\Delta H/H_s)$$

Figure 5-2 Chart for Reduction of "During Test" Data

Table 5-1 Schedule of Tests

Test	Soil	Apparatus	Sequence #	Start Date	Stop Date
A	EPKW	II	1	28 SEP 84	3 NOV 84
B	EPKW	III	1	31 JAN 85	27 FEB 85
C	EPKW	III	4	27 MAR 85	18 APR 85
D	NOVW	II	5	1 MAR 85	20 MAR 85
E	NOVW	II	7	4 APR 85	19 APR 85
F	NOVW	III	3	12 MAR 85	27 MAR 85

Table 5-2 Specimen Data

	Units	Test → A Soil → EPKW	B EPKW	C EPKW	D NOVW	E NOVW	F NOVW
w	%	37.22	40.43	43.64	20.97	20.97	20.97
W	g	182.42	173.87	170.58	172.35	173.71	184.19
d	cm	7.600	7.617	7.736	7.683	7.747	7.722
	in	2.992	2.999	3.046	3.025	3.050	3.040
H	cm	2.226	2.245	2.197	2.041	2.098	2.229
	in	0.876	0.884	0.865	0.804	0.826	0.878
G_s		2.59	2.59	2.59	2.65	2.65	2.65
A	cm^2	45.359	45.573	47.003	46.361	47.136	46.827
	in^2	7.030	7.064	7.285	7.186	7.306	7.258
V	cc	100.968	102.326	103.265	94.622	98.892	104.377
	in^3	6.161	6.244	6.302	5.774	6.035	6.369
V_s	cc	47.023	47.804	45.851	53.764	54.188	57.457
	in^3	2.870	2.917	2.798	3.281	3.307	3.506
H_s	cm	1.081	1.049	0.976	1.160	1.150	1.227
	in	0.426	0.413	0.384	0.457	0.453	0.483
e_o		1.0232	1.1405	1.2522	0.7600	0.8250	0.8166
γ	g/cc	1.807	1.699	1.652	1.821	1.757	1.765
B		1.000	0.952	1.000	1.000	0.940	1.000

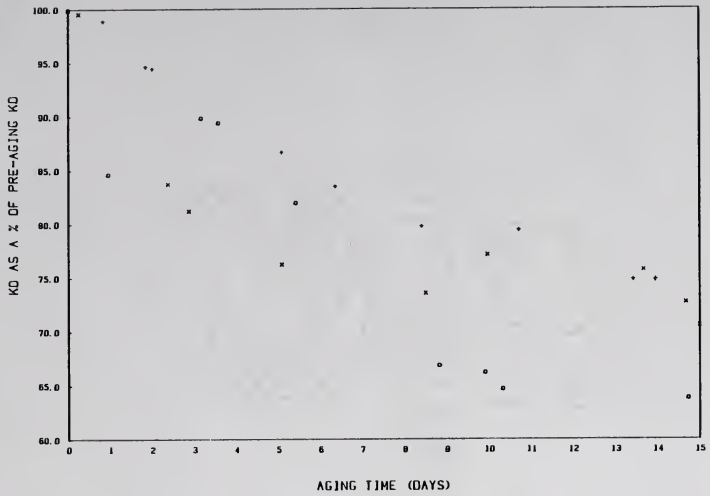

Figure 5-3 Tests A, B and C: K_o as a % of Pre-Aging K_o with Time (Test A = o; Test B = x; Test C = +)

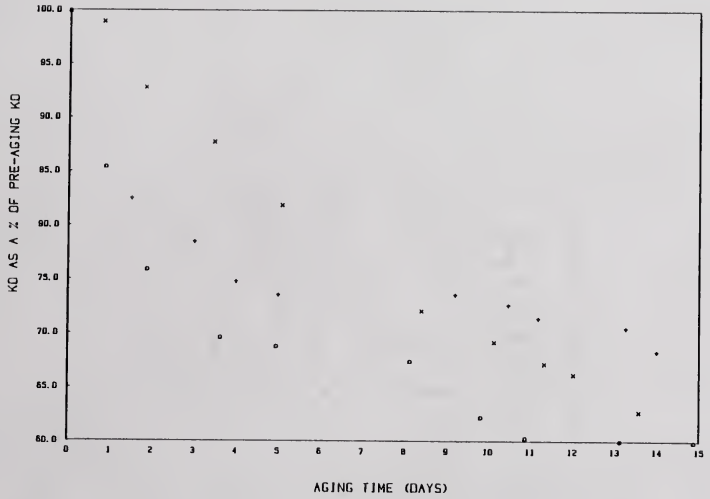

Figure 5-4 Tests D, E and F: K_o as a % of Pre-Aging K_o with Time (Test D = o; Test E = +; Test F = x)

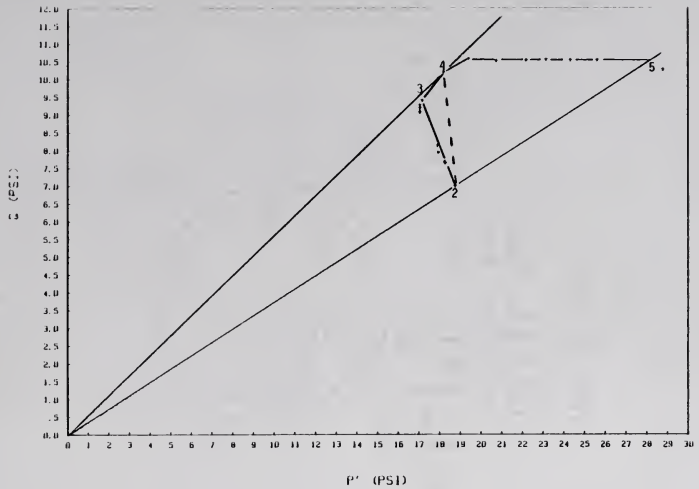

Figure 5-5 Test A: p'-q Diagram with Schmertmann Quantitative Theory Notation

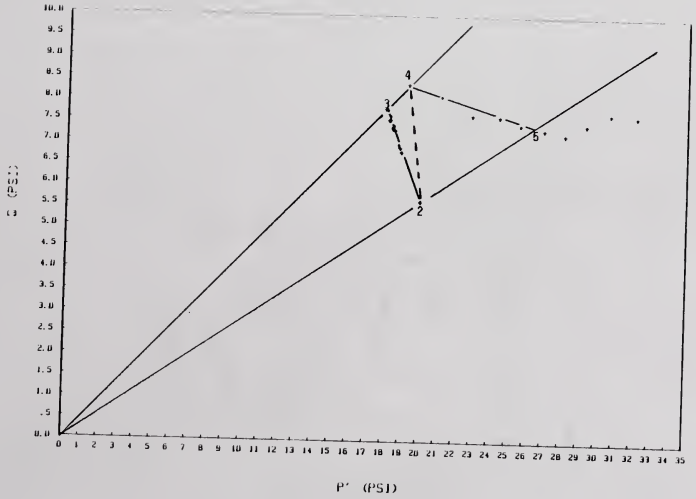

Figure 5-6 Test B: p'-q Diagram with Schmertmann Quantitative Theory Notation

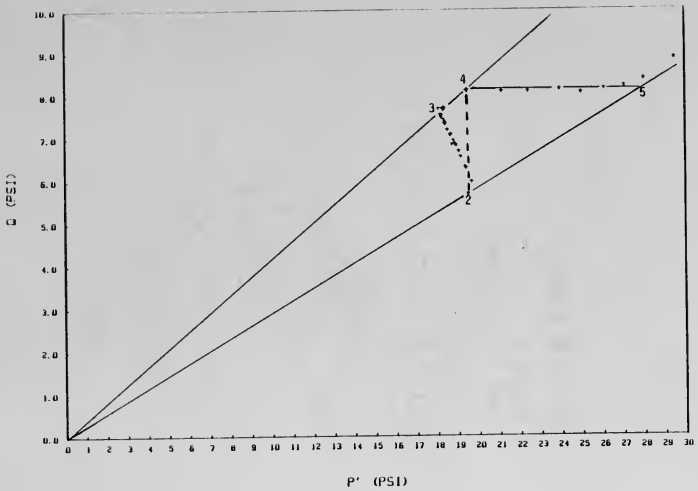

Figure 5-7 Test C: p'-q Diagram with Schmertmann Quantitative Theory Notation

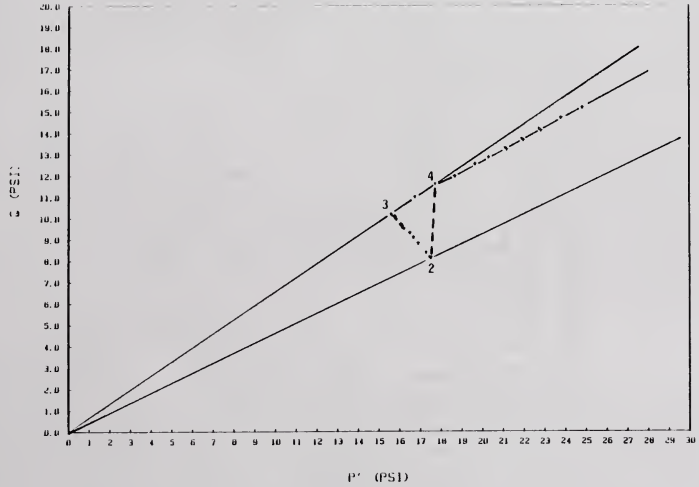

Figure 5-8 Test D: p'-q Diagram with Schmertmann Quantitative Theory Notation

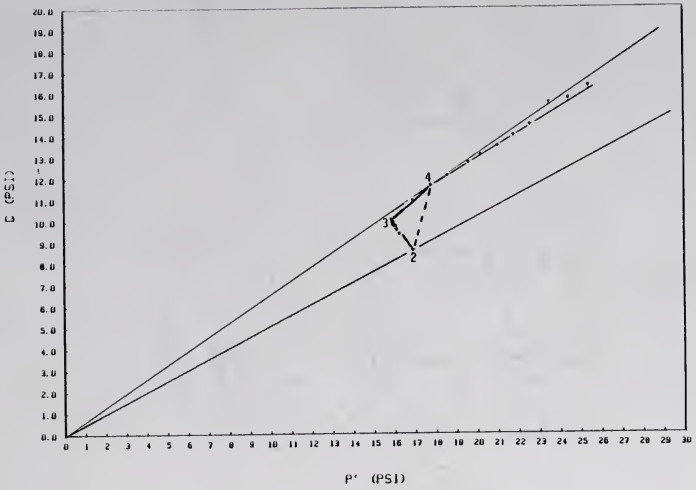

Figure 5-9 Test E: p'-q Diagram with Schmertmann Quantitative Theory Notation

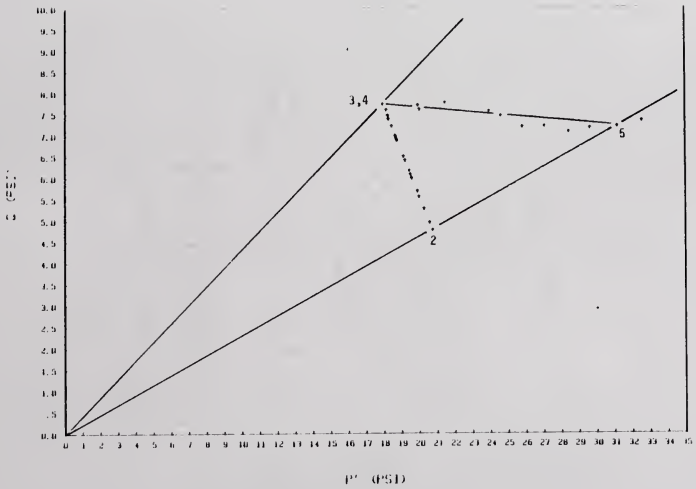

Figure 5-10 Test F: p'-q Diagram with Schmertmann Quantitative Theory Notation

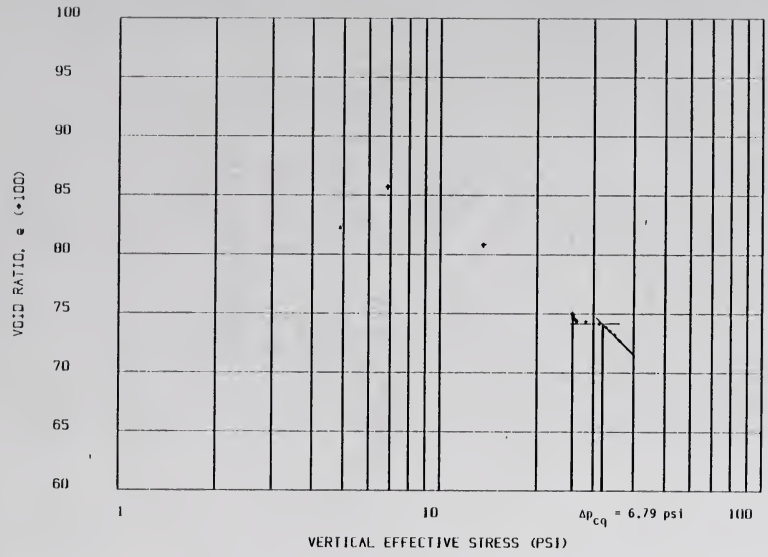

Figure 5-11 Test A: e-log σ_1' Plot with q-p_c Effect Noted

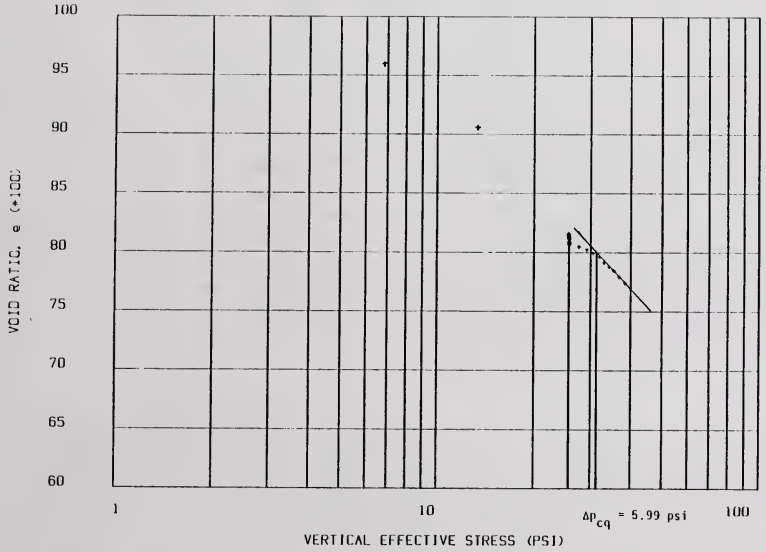

Figure 5-12 Test B: e-log σ'_1 Plot with q-p_c Effect Noted

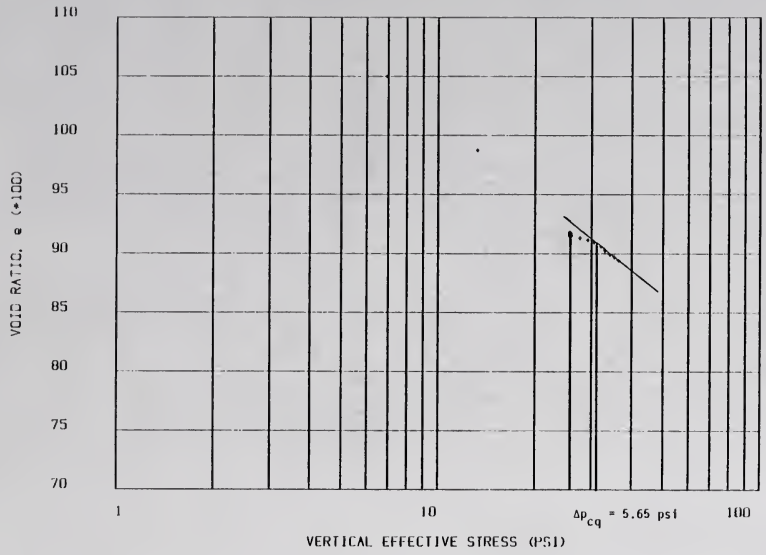

Figure 5-13 Test C: e-log σ_1' Plot with q-p_c Effect Noted

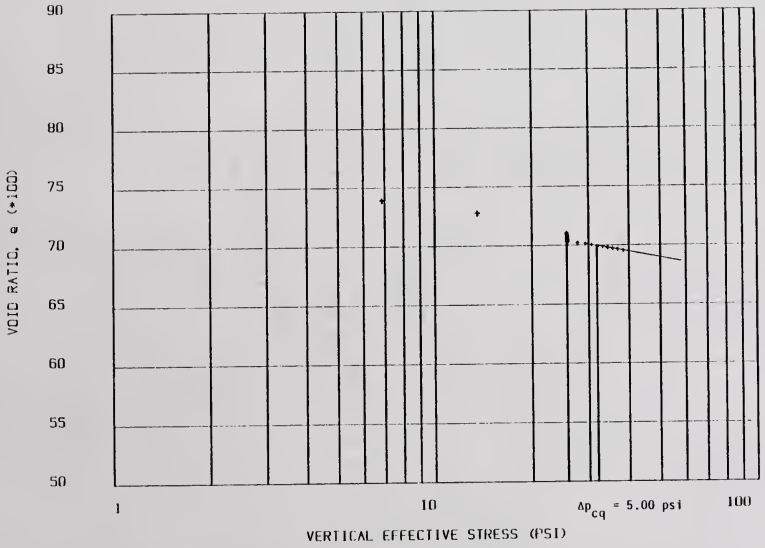

Figure 5-14 Test D: e-log σ_1' Plot with q-p_c Effect Noted

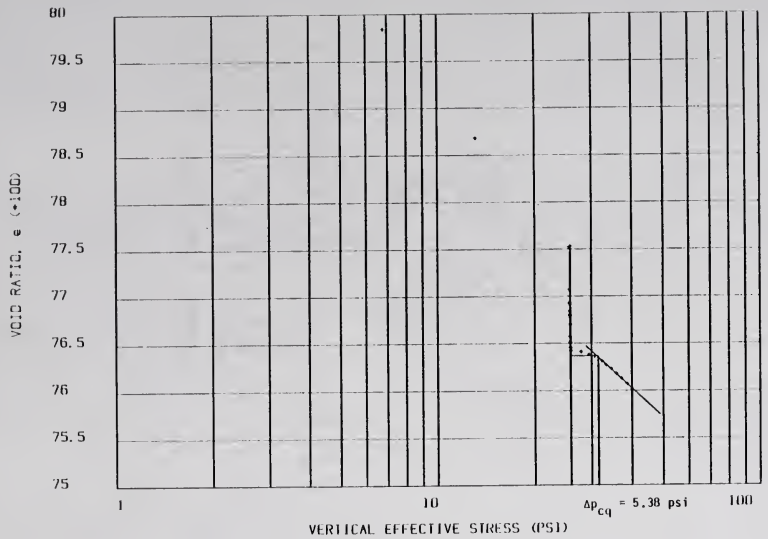

Figure 5-15 Test E: e-log σ_1' Plot with q-p_c Effect Noted

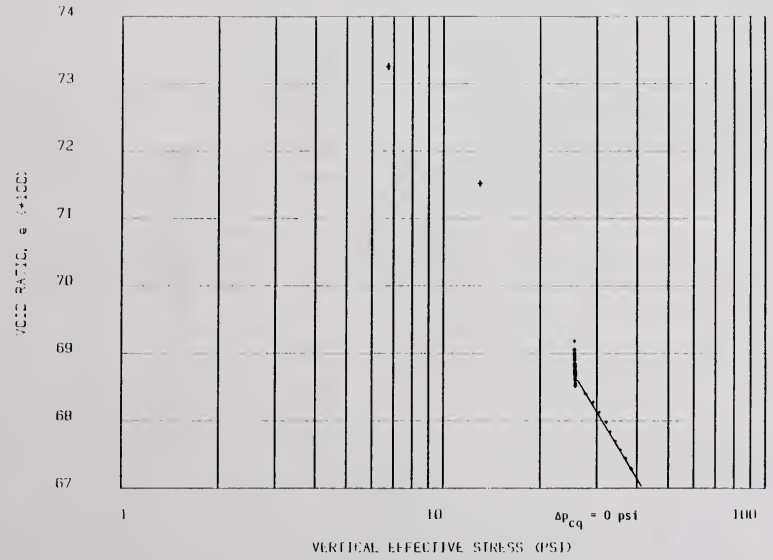

Figure 5-16 Test F: e-log σ_1' Plot with q-p_c Effect Noted

Table 5-3 Summary of K_o and e Information

	Units	Test → A	B	C	AVG	D	E	F	AVG
Soil →		EPKW	EPKW	EPKW	EPKW	NOVW	NOVW	NOVW	NOVW
Aging Time	days	14.717	17.302	13.975	-	14.875	13.990	13.573	-
Reduction in K_o During Aging	%	36.10	29.89	24.26	30.08	43.17	31.69	37.18	37.43
Pre-Aging K_o	-	.457	.562	.540	-	.366	.325	.632	-
Post-Aging K_o	-	.292	.394	.409	-	.208	.222	.397	-
Pre-Aging ϕ [ϕ = arcsin(1-K_o)]	deg.	32.89	25.98	27.39	28.75	39.34	42.45	21.59	40.90
Post-Aging ϕ [ϕ = arcsin(1-K_o)]	deg.	45.07	37.30	36.23	39.53	52.37	51.08	37.08	51.72
Increase in ϕ during aging	deg.	12.18	11.32	8.84	10.78	13.03	8.63	15.49	10.82
Reduction in e, 0 → 3 (Primary and Secondary Compression)	-	.2797	.3336	.3375	-	.0574	.0608	.1315	-
	%	27.34	29.25	26.95	27.85	7.55	7.37	16.11	7.46
Reduction in e, 3 → END (Small Loads)	-	.0256	.0380	.0340	-	.0081	.0048	.0138	-
	%	2.50	3.33	2.72	2.85	1.07	0.58	1.69	0.82

Table 5-4 Summary of q-p_c Effect Calculations

Test	p_o[a] (psi)	S_2[b]	S_4[c]	A_q[d]	Δp_{cq}[e] (psi)	Δp_{cq} from e-log σ_1' plot (psi)	Δp_{cq} theory/p_o (%)	Δp_{cq} plot/p_o (%)	Prediction by Quantitative Theory Over (%)	Under (%)
A	25.63	.373	.560	.588	2.62	6.79	10.22	26.49		16.27
B	25.63	.280	.436	.640	2.00	5.99	7.80	23.37		15.57
C	25.63	.299	.417	.504	2.30	5.65	8.97	22.04		13.07
D	25.63	.464	.656	.632	2.11	5.00	8.23	19.51		11.28
E	25.63	.509	.656	.356	3.96	5.38	15.45	20.99		5.54
F	25.63	.225	.432	.981	0.12	0	0.47	0	0.47	

[a] $p_o = \sigma_1'$ = the normal consolidation pressure.

[b] S_2 = the slope of the initial K_o-line = $(1-K_o$ @ point 2$)/(1+K_o$ @ point 2).

[c] S_4 = the slope of the K_o-line after the q-p_c effect = $(1-K_o$ @ point 4$)/(1+K_o$ @ point 4).

[d] A_q = the net effect of A over the entire 2-4 ESP of the q-p_c process.

$$A_q = \frac{p_2'-p_4'+q_4-q_2}{2(q_4-q_2)}$$ = empirically derived expression which replaced the less general expression reported by Schmertmann (1981). The latter expression for A_q was based on the assumptions that point 3 (Figure 2-1) did not lie on the slope S_4 and ESP 3-4 occurred at A=0.

[e] $$\Delta p_{cq} = \frac{2(1-A_q)(S_4-S_2)}{[1(1-2A_q)S_4](1+S_2)}$$ = the magnitude of the q-p_c effect using Schmertmann's theory.

CHAPTER 6
DISCUSSION AND SUMMARY OF RESULTS

6.1 Introduction

Chapter 6 evaluates the test results presented in the previous chapter and the performance of the UF K_o-consolidometer during the tests. Sections 6.2 and 6.3 offer answers to the K_o-behavior and quantitative theory questions posed in Section 1.2. Section 6.4 examines the performance of the UF K_o-consolidometer in light of the criteria defined in Chapter 4. Section 6.5 addresses questions considered by the UF research team and likely to arise in a critical review of this study. Finally, Section 6.6 summarizes these dicussions.

Prior to further discussions, some comments on Test F seem appropriate. Noting Figure 5-10, Figure 5-16, Table 5-3 and Table 5-4, the reader easily determines Test F results are inconsistent with Tests D and E. The obvious question is why. Perusal of the specimen data and laboratory notes suggest no procedural or equipment deficiencies. Moreover, the laboratory notes indicate no sample disturbance during testing. However, the low pre-aging friction angle and large changes in void ratio indicate the sample may have been disturbed. Consequently, the Test F results were not used in determining NOVW characteristics. Nevertheless, Test F results are

important to this study because they allow the evaluation of the quantitative prediction theory for the $\Delta p_{cq} = 0$ case.

6.2 K_o-Behavior During Secondary Compression Aging

6.2.1 Discussion

As previously noted in Section 1.2, this study sought to answer how K_o behaves during secondary aging in one-dimensional compression for NC fine-grained soils. Figure 5-3, Figure 5-4, and Table 5-3 summarize the information gathered during this project to answer that question.

K_o-values for the EPKW specimens decreased an average of 30.08% over a nominal 15-day aging period. K_o-values for the NOVW specimens decreased an average of 37.43% over the same period.

Friction angle values (ϕ) were calculated using pre-aging and post-aging K_o-values in Jaky's Equation [$\phi = \arcsin(1-K_o)$]. The average pre-aging ϕ values were 28.75° and 40.90° for EPKW and NOVW, respectively. Due to the decrease in K_o, corresponding friction angle values increased during aging. Both EPKW and NOVW averaged an increase in ϕ of 10.8°.

6.2.2 Summary

For each of the six tests on NC fine-grained soil, K_o decreased during secondary aging in one-dimensional compression. The average magnitude of decrease was 30.08% and 37.43% for EPKW and NOVW, respectively.

6.3 Quantitative Prediction of the q-p_c Effect

6.3.1 Discussion

The second question this study examined was the accuracy of the assumptions and predictions of the existing quantitative theory for predicting the q-p_c effect (Schmertmann, 1981).

As discussed in Section 2.3, Schmertmann's quantitative theory formula was derived from an assumed stress path predicated on his soil friction-increase theory. If the stress paths for the six tests (Figures 5-5 through 5-10) match the assumed stress path (Figure 2-1), then his assumptions and soil friction-increase theory would be validated. From studying Figures 5-5 through 5-10, the author suggests the six tests validate the initial 2-3 portion of the stress path. However, the 3-4 portion of the path occurred at a somewhat lower slope than Schmertmann's A=0 line. In most tests, the 3-4 portion was almost along the S_4 line. Therefore, the slope A_q required in the prediction equation was calculated as described in Table 5-4 and illustrated in Appendix H, rather than using the equation derived by Schmertmann which was based on the assumed ESP discussed in Section 2.3.2. Moreover, with the previously noted exception of Test F, the NOVW specimens do not readily return to the initial K_o-line, as do the EPKW specimens, under the small loads applied. This occurrence indicates the aging effect is more difficult to destroy in the NOVW. The shape of the stress paths and the need for additional loading to destroy the aging effect in the material of greater friction support the soil friction-increase

theory and thus the assumptions underlying the quantitative theory formula.

The next step was to examine the capability of the derived mathematical expression to accurately predict the q-p_c effect. As shown in Figure 2-1, the magnitude of the q-p_c effect may be obtained graphically from an e-log σ_1' plot. For purposes of evaluation, values computed from Schmertmann's expression were compared to those obtained graphically from Figures 5-11 through 5-16. These values for Δp_{cq} were then divided by the consolidation pressure p_o to compute the percentage of additional load which could be carried due to the q-p_c effect. Table 5-4 summarizes the q-p_c effect calculations.

To achieve a common basis for comparison, the author defined the end of the q-p_c effect as the first departure from the post-aging slope S_4 and the first departure from a straignt line through the small load void ratios for the mathematical and graphical techniques, respectively. Clearly, the entire aging effect is not destroyed until the stress path returns to the original K_o-line and some analysts may include points beyond the first departure in the q-p_c effect. This caveat should aid the reader in following the author's analysis.

Schmertmann's quantitative theory predictions underpredicted graphical values by an average of 14.97% for the three EPKW tests. The average value for $\Delta p_{cq}/p_o$ for EPKW was 9.00% and 23.97% using the mathematical and graphical procedures, respectively.

Average mathematical and graphical $\Delta p_{cq}/p_o$ values for NOVW, based on Tests D and E, were 11.84% and 20.25%, respectively. As

mentioned in Section 6.1, Test F was analyzed to determine if the Schmertmann expression was valid when $\Delta p_{cq}/p_o$ was known to be zero. The Schmertmann expression is general enough to predict $\Delta p_{cq} = 0$ when the $q\text{-}p_c$ effect has been destroyed.

The differences expressed above are a consequence of the procedures chosen to define the number 4 points on the p'-q diagrams, Figures 5-5 through 5-10, and on the e-log σ_1' plots, Figures 5-11 through 5-16.

6.3.2 Summary

The shape of the stress paths and the need for additional loading to destroy the aging effect in the material of greater particle friction, NOVW, support the soil friction-increase theory and thus the assumptions underlying Schmertmann's quantitative theory for the $q\text{-}p_c$ effect. Schmertmann's quantitative theory predictions underpredicted graphical values from the e-log σ_1' plots by an average of 14.97% for EPKW and 8.41% for NOVW. Both prediction methods are subject to the analyst's judgment.

6.4 Equipment Performance Evaluation

6.4.1 Discussion

General. During the six tests, the UF K_o-consolidometer performed well each function described in Chapter 4. This section examines the two subsystems whose level of performance may be measured in numerical terms based on test data. Excluding the friction characteristics of the test cell which will be discussed in

Section 6.5, the performance of the other six subsystems is measured qualitatively as functional or dysfunctional. Each of these six were functional throughout the testing program.

Volume Change Measurement Subsystem (VCMS). The function of the VCMS is to drain water. Moreover, the VCMS provides a check on the mercury manometer since the water expelled from the specimen should equal the vertical change in specimen height times the specimen area for the K_o-condition. The primary function of draining water was easily achieved. However, an extensive investigation was necessary when the agreement between the mercury manometer and the VCMS began deviating after primary consolidation in each test due to water loss in the VCMS.

The first step was to insure water was not "backing up" into the specimen during aging. If this occurred, the constant volume necessary to maintain the K_o-condition would be compromised. Sealing off the chamber from the rest of the system (both by valve and removal), the research team found the water loss still continued, thus eliminating "backing up" as the source of loss.

Step 2 was to insure water was not being lost through leakage. Both the Mark II and Mark III systems were charged with freon at 80 psi pressure and checked for leaks. No leaks were found in either VCMS.

Pursuant to the co-principal investigator's suggestion that temperature could contribute to water loss, the research team installed a new heater in the temperature control room. Although this reduced the maximum temperature variation from ±2°F to ±0.3°F,

the water losses continued. Therefore, temperature effects on the VCMS seemed negligible.

Eliminating "back up," leakage, and temperature as possible causes, the investigation turned to time-related phenomena--evaporation and absorption. In an attempt to prevent evaporation and absorption, an oil cover was placed on top of the water in the small buret and nylon tubing was replaced with copper tubing where possible. Despite these efforts, the VCMS continued to lose water.

In Step 5, a series of tests were conducted at various backpressures to develop water loss calibrations for each VCMS. However, the only consistent trend in the data was that the volume loss rate increased with each subsequent event on the system, regardless of pressure.

Finally, the research team took the data to Dr. David E. Clark, a professor in the UF Department of Materials Science and Engineering and a specialist in the environmental sensitivity of materials and the properties of glass. Dr. Clark made the following statements concerning water loss in the VCMS:

1) Absorption and evaporation do occur through nylon tubing. The rate of absorption/evaporation is a function of humidity and the permeability of the material.
2) The trend of increased volume loss is consistent with decreased humidity due to the laboratory air conditioner being used more as the semester progresses.

3) The trend of increased volume loss is also consistent with increased permeability of the lines resulting from age and environmental interaction.

4) Some of the water lost may be absorbed by hydrated products formed inside the copper tubing due to basic nature of the water expelled from the EPKW specimens.

To sum up, the VCMS still performs its basic function of draining water. The secondary function of providing a check for the mercury manometer is achieved until the end of primary consolidation. At this point, the absorption/evaporation of water through the nylon tubing, masked by large volumes during primary consolidation, appears as a drop in the VCMS. These losses do not affect the maintenance of the K_o-condition, the operation of other subsystems, or the validity of the test.

Temperature Control Subsystem (TCS). The function of the TCS is to maintain a constant temperature. As mentioned in the preceding discussion, the capability of the TCS was improved by replacing the former heat source with the Arvin portable electric heater, previously discussed and shown in Figure 4-14. This equipment was installed during Test B. Consequently, the mean temperature variations for Tests A and B are greater than those for Tests C through F as shown in Table 6-1. In sum, the temperature information provided in Table 6-1 reveals the TCS successfully maintained a constant temperature.

Table 6-1 Temperature Control Subsystem (TCS) Data

	Units	Test → A	B	C	D	E	F
Desired Temperature	°F	83.5	80.1	80.1	80.1	80.1	80.1
Maximum Deviation Above Desired Temperature	°F	1.2	0.8	0.5	0.3	0.5	0.6
Maximum Deviation Below Desired Temperature	°F	3.6	3.8	0.1	1.1	0.1	0.1
Mean Deviation Above Desired Temperature	°F	0.4	0.2	0.2	0.1	0.2	0.1
Mean Deviation Below Desired Temperature	°F	0.6	1.5	0.1	0.2	0.1	0.1

6.4.2 Summary

The UF K_o-consolidometer performed each primary function for which it was designed. A water loss in the VCMS due to absorption/evaporation in the nylon tubing prevented the secondary function of mercury manometer checks beyond primary consolidation. This water loss did not compromise the K_o-condition or the validity of the tests. The TCS was successful in maintaining a constant temperature for each test.

6.5 Questions/Answers Regarding Results

6.5.1 Discussion

This section addresses three questions considered by the UF research team and likely to arise in a critical review of this study.

1) QUESTION: Is the test cell piston subject to horizontal eccentricity which would reduce the vertical stress felt by the specimen and thus alter K_o?

ANSWER: First, the UF K_o-consolidometer test cell was designed to preclude horizontal eccentricity on the piston. As discussed in Section 4.3.1, load is transmitted to the piston via a press-fitted rod which rides in two Thomson stainless steel linear ball bushings. Two sets of bushings were used to eliminate eccentricity.

Second, an experiment was conducted to insure the ball bushings were doing their job. A string was tied around the rod, run over a pulley, and loaded with weights to put a

horizontal load on the rod and thus the piston. At each horizontal load, the vertical load necessary to make the piston move was measured. Apparently the ball bushings work quite well, since the piston moved under its own weight for potential eccentricities up to 112%, where the experiment ended (Table 6-2).

2) QUESTION: Since the test cell has no load cell for the measurement of vertical stress, how reliable are the results of this study?

ANSWER: Clearly, this question would not be posed if funds had been available to equip the test cells with load cells when constructed. Using observation, calibration, and parametric studies, the research team determined the role of piston friction in altering the vertical stress.

If piston friction was building with time, logic dictates the dial readings should reflect the change in piston movement. For example, if the piston stopped, then the dial readings would remain constant. Moreover, if the piston stopped then started again after overcoming friction, dial readings would reflect a constant period followed by an abrupt change. Instead, the dial readings show a consistent decrease in height of the specimen, characteristic of secondary compression.

Table 6-3 gives the piston friction data for the Mark II and Mark III test cells. The cells were filled with

Table 6-2 Investigation of Eccentricity Effects in Test Cell

Horizontal Load, g	Vertical Load to Move Piston, g	Eccentricity = Horiz. Load / Vert.Load @ Horiz.Load=0
0	1611.2 (Piston Weight)	0
70.6	1611.2	4.38
170.6	1611.2	10.59
270.6	1611.2	16.79
370.6	1611.2	23.00
470.6	1611.2	29.21
570.6	1611.2	35.41
1811.9	1611.2	112.46

Table 6-3 Piston Friction Data

	Units	Mark II Test Cell			Mark III Test Cell		
Simulated Backpressure	psi	17.50	33.62	61.18	16.92	32.83	61.18
Piston Friction	psi	0.08	0.16	0.33	0.20	0.13	0.56
Consolidation Pressure p_o	psi	25.63	25.63	25.63	25.63	25.63	25.63
Total Vertical Stress for p_o at Simulated Backpressure	psi	43.13	59.25	86.81	42.55	58.46	86.81
Piston Friction/ Total Vertical Stress	%	0.18	0.27	0.38	0.47	0.22	0.64

water, placed in their respective oedometer, and pressurized to simulate operational backpressures. After balancing the load arm to counteract uplift, the weight necessary to move the piston was measured. Knowing the loading arm ratio and the cross-sectional area of the piston, this load was converted into a pressure expression for piston friction. Finally, piston friction is expressed as a percentage of the total vertical stress necessary to establish a consolidation pressure of 25.63 psi at the simulated backpressure. This table shows the piston friction is negligible.

Table 6-4 offers a parametric study of piston friction using a "typical" point from Test D. The parametric study confirms K_o is sensitive to piston friction. However, the study also reveals high percentages of piston friction would be required to compute K_o values that remain constant or increase from the start of aging, given the σ'_3 value.

In conclusion, implementing a load cell is the ultimate answer to monitoring the vertical stress and piston friction. However, observation, calibration, and parametric studies indicate the total vertical stress remains constant and free from piston friction effects throughout the test.

3) QUESTION: How accurately was the operator able to maintain the K_o-condition using the mercury manometer?

ANSWER: The UF K_o-consolidometer was monitored every 2 to 4 hours for the duration of the test. Adjustments were made in small increments, as indicated by the manometer, to

Table 6-4 Parametric Study of Piston Friction Using a "Typical" Point from Test D

Data: Aging time = 7.917 days
σ_1 = 42.47 psi
u = 16.16 psi
σ_3 = 22.97 psi

Reduction in K_o Since Start of Aging = 33.33%

K_o at Start of Aging = .366

% Decrease Due to Friction	σ_1	σ'_1	σ'_3	K_o	% Increase in K_o
0	42.47	25.80	6.30	.244	0
1	42.04	25.37	6.30	.248	1.64
2	41.62	24.95	6.30	.252	3.28
3	41.20	24.53	6.30	.257	5.33
4	40.77	24.10	6.30	.261	6.97
5	40.35	23.68	6.30	.266	9.02
6	39.92	23.25	6.30	.271	11.06
7	39.50	22.83	6.30	.276	13.11
8	39.07	22.40	6.30	.281	15.16
9	38.65	21.98	6.30	.287	17.62
10	38.22	21.55	6.30	.292	19.67
15	36.10	19.43	6.30	.324	32.79
16	35.67	19.00	6.30	.332	35.89
17	35.25	18.58	6.30	.339	38.93
20.2	33.88	17.21	6.30	.366	50.00

maintain the K_o-condition. Table 6-5 gives the mean for readings above and below the K_o-level for each test. These data suggest an experienced operator can successfully maintain the K_o-condition using the mercury manometer as an indicator of lateral strain.

6.5.2 Summary

The UF K_o-consolidometer test cell exhibited no horizontal eccentricity of the piston when tested. Moreover, piston friction appeared negligible based on observation and calibration of both test cells. Test data suggest an experienced operator can successfully maintain the K_o-condition using the mercury manometer as an indicator of lateral strain.

6.6 Summary

This chapter addressed a broad range of issues regarding the test results and equipment performance. The statements below summarize the discussions on these issues.

1) K_o decreased an average of 30.08% and 37.43% for normally consolidated EPKW and NOVW specimens, respectively, during secondary aging in one-dimensional compression.
2) Both EPKW and NOVW specimens exhibited the q-p_c effect. Schmertmann's quantitative theory predictions for the q-p_c effect underpredicted graphical values by an average of 14.97% for EPKW and 8.41% for NOVW.

Table 6-5 Operation of the Lateral Strain Null Subsystem (LSNS) or Mercury Manometer

	Units	Test → A	B	C	D	E	F
Mean Deviation Above K_o-Level	psi	0.18	0.09	0.03	0.05	0.10	0.03
Mean Deviation Below K_o-Level	psi	0.18	0.05	0.03	0.04	0.05	0.03

3) The UF K_o-consolidometer performed each primary function for which it was designed. The only problem area was the water loss from the VCMS after primary consolidation. This loss, due to absorption/evaporation in the nylon tubing, prevented checks on the mercury manometer after primary consolidation but did not compromise the K_o-condition or the validity of the tests.

4) Eccentricity and friction in the piston do not appear to be factors in the UF K_o-consolidometer test cells. Performance data suggest an experienced operator can successfully maintain the K_o-condition using the mercury manometer as an indicator of lateral strain.

CHAPTER 7
CONCLUSIONS AND RECOMMENDATIONS

7.1 Conclusions

Analysis of the test results and equipment performance for the six K_o-consolidation tests on NC fine-grained soils appears to justify the following conclusions.

1) K_o decreases during secondary aging in one-dimensional compression for NC fine-grained soils.
2) The $q\text{-}p_c$ effect develops in both cohesive and cohesionless fine-grained soils. Moreover, greater loads are required to destroy the aging effect in the cohesionless soil. Both occurrences suggest the $q\text{-}p_c$ effect develops due to increased friction rather than bonding.
3) Schmertmann's quantitative theory predictions for the $q\text{-}p_c$ effect underpredict graphical values by an average of 14.97% for EPKW and 8.41% for NOVW. This agreement is reasonable considering the subjective aspects of both techniques.
4) The UF K_o-consolidometers are capable of maintaining and accurately measuring the K_o-condition when operated by experienced people using the prescribed techniques.

7.2 Recommendations

The author offers the following suggestions for furthering this research.

1) Pursue current UF plans to implement a load cell into the test cell. This action would eliminate the need for piston friction calibration.
2) Expand the data base. More tests on EPKW and NOVW should be run to provide additional evidence for the previously stated conclusions. Moreover, tests should be run on other NC fine-grained soils to verify the findings.
3) Invite other researchers to UF to review the equipment and test specimens of their choice. Based on the diversity of opinion found during the literature review, the author thinks this may be the only way to settle the arguments surrounding K_o-behavior and the origins of the q-p_c effect.

APPENDIX A
TEST A: TABULATED RESULTS AND RAW PLOTS

Table A-1 Test A: Values for t, K_o, p', q, and K_o in %

Aging Time t (days)	K_o	p' (psi)	q (psi)	K_o as % of Pre-Aging K_o
0	.457	18.76	7.00	100
.944	.387	17.94	7.94	84.68
3.153	.411	18.29	7.64	89.94
3.569	.409	18.26	7.66	89.50
5.410	.375	17.90	8.13	82.06
8.819	.306	17.05	9.07	66.96
9.900	.303	17.06	9.19	66.30
10.319	.296	17.06	9.27	64.77
14.717	.292	17.18	9.40	63.90
	.282	18.20	10.20	
	.294	19.41	10.58	
	.327	20.74	10.52	
	.356	22.18	10.54	
	.374	23.13	10.55	
	.395	24.32	10.54	
	.417	25.61	10.54	
	.475	28.78	10.26	

Table A-2 Test A: Values for σ_1', e, e in %, σ_3', and u

σ_1' (psi)	e	e as % of initial e	σ_3' (psi)	u (psi)
6.81	.8566	83.72		
13.29	.8084	79.01		
25.76	.7506	73.36	11.77	60.55
25.87	.7487	73.17	10.00	60.44
25.92	.7464	72.95	10.65	60.39
25.92	.7461	72.92	10.60	60.39
26.02	.7461	72.92	9.76	60.29
26.12	.7459	72.90	7.98	60.19
26.36	.7454	72.85	7.99	59.95
26.32	.7454	72.85	7.79	59.99
26.59	.7435	72.66	7.78	59.72
28.39	.7433	72.64	8.00	59.89
29.99	.7417	72.49	8.83	59.87
31.26	.7414	72.46	10.22	59.90
32.71	.7386	72.13	11.64	60.01
33.67	.7356	71.89	12.58	60.01
34.85	.7323	71.57	13.78	60.08
36.15	.7273	71.08	15.07	60.04
39.03	.7179	70.16	18.52	60.02

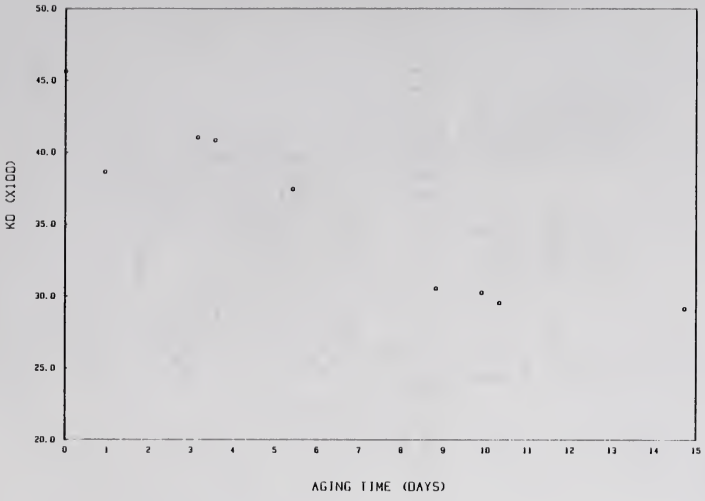

Figure A-1 Test A: K_o with Aging Time

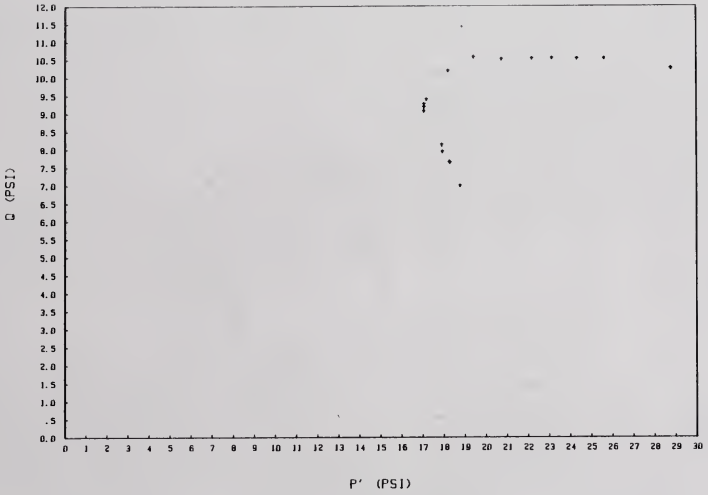

Figure A-2 Test A: p'-q Diagram

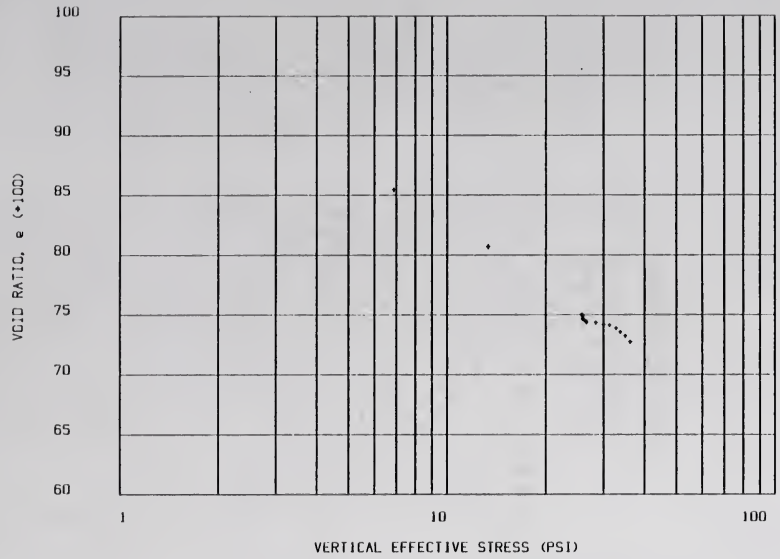

Figure A-3 Test A: e-log σ_1' Plot

APPENDIX B
TEST B: TABULATED RESULTS AND RAW PLOTS

Table B-1 Test B: Values for t, K_o, p', q, and K_o in %

Aging Time t (days)	K_o	p' (psi)	q (psi)	K_o as % of Pre-Aging K_o
0	.562	19.98	5.63	100
.167	.561	19.98	5.63	99.82
.250	.560	19.98	5.63	99.64
2.375	.471	18.87	6.79	83.81
2.667	.471	18.85	6.79	83.81
2.875	.457	18.69	6.96	81.32
4.149	.464	18.79	6.89	82.56
4.233	.463	18.78	6.89	82.38
5.083	.429	18.34	7.34	76.33
6.035	.412	18.15	7.55	73.31
6.667	.426	18.33	7.37	75.80
6.854	.430	18.39	7.33	76.51
7.000	.430	18.38	7.33	76.51
7.333	.426	18.34	7.39	75.80
8.250	.414	18.20	7.55	73.66
8.500	.414	18.20	7.55	73.66
9.969	.434	18.47	7.30	77.22
12.250	.412	18.12	7.54	73.31
13.000	.434	18.51	7.31	77.22
13.500	.422	18.35	7.45	75.09
13.667	.426	18.41	7.41	75.80
14.500	.405	18.14	7.68	72.06
14.667	.409	18.20	7.64	72.78
15.167	.397	18.04	7.79	70.64
17.302	.394	17.94	7.80	70.11
	.393	19.21	8.38	
	.444	21.05	8.11	
	.498	22.83	7.66	
	.523	24.36	7.64	
	.548	25.55	7.46	
	.571	26.90	7.34	
	.590	28.08	7.23	
	.593	29.28	7.47	
	.598	30.63	7.73	
	.614	32.13	7.68	

Table B-2 Test B: Values for σ_1', e, e in %, σ_3', and u

σ_1' (psi)	e	e as % of initial e	σ_3' (psi)	u (psi)
6.86	.9594	84.12		
13.18	.9059	79.43		
25.60	.8160	71.55	14.39	16.87
25.60	.8160	71.55	14.35	16.87
25.61	.8159	71.54	14.35	16.86
25.65	.8148	71.44	12.08	16.82
25.63	.8146	71.42	12.06	16.84
25.65	.8146	71.42	11.73	16.82
25.67	.8132	71.30	11.90	16.80
25.67	.8131	71.29	11.89	16.80
25.69	.8129	71.28	11.02	16.78
25.70	.8122	71.21	10.60	16.77
25.70	.8121	71.20	10.96	16.77
25.72	.8121	71.20	11.06	16.75
25.71	.8121	71.20	11.05	16.76
25.73	.8120	71.20	10.95	16.74
25.74	.8117	71.17	10.65	16.73
25.74	.8116	71.16	10.65	16.73
25.76	.8112	71.13	11.17	16.71
25.65	.8086	70.90	10.58	16.82
25.81	.8085	70.89	11.20	16.66
25.80	.8085	70.89	10.90	16.67
25.81	.8085	70.89	11.00	16.66
25.81	.8082	70.86	10.46	16.66
25.83	.8082	70.86	10.56	16.64
25.82	.8081	70.85	10.25	16.65
25.74	.8069	70.75	10.14	16.73
27.59	.8049	70.57	10.83	16.85
29.16	.8025	70.36	12.94	16.86
30.49	.7994	70.09	15.17	16.83
31.99	.7963	69.82	16.72	16.89
33.01	.7914	69.39	18.09	16.83
34.25	.7877	69.06	19.54	16.84
35.31	.7847	68.80	20.85	17.04
36.75	.7791	68.31	21.81	16.90
38.34	.7741	67.87	22.88	16.91
39.31	.7689	67.42	24.45	16.91

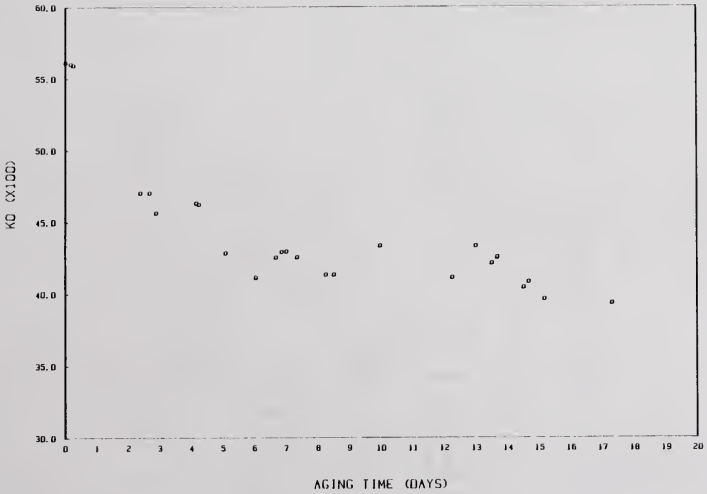

Figure B-1 Test B: K_o with Aging Time

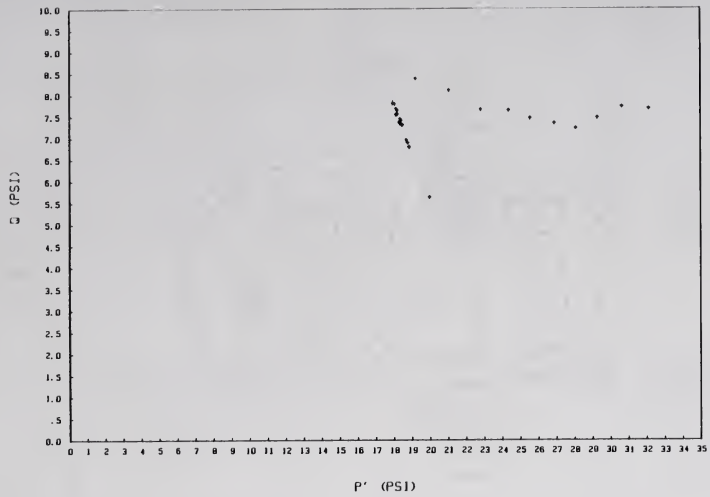

Figure B-2 Test B: p'-q Diagram

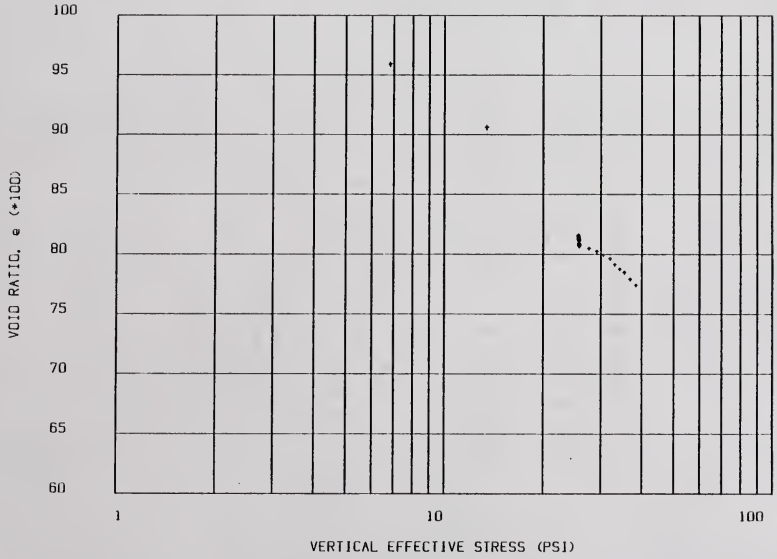

Figure B-3 Test B: e-log σ_1' Plot

APPENDIX C
TEST C: TABULATED RESULTS AND RAW PLOTS

Table C-1 Test C: Values for t, K_o, p', q, and K_o in %

Aging Time t (days)	K_o	p' (psi)	q (psi)	K_o as % of Pre-Aging K_o
0	.540	19.50	5.68	100
.833	.534	19.67	5.97	98.89
1.430	.507	19.36	6.32	93.89
1.848	.511	19.41	6.29	94.63
2.010	.510	19.40	6.29	94.44
3.000	.491	19.16	6.55	90.92
4.104	.481	19.06	6.68	89.07
4.510	.470	18.94	6.82	87.04
4.840	.468	18.87	6.84	86.67
5.081	.468	18.89	6.85	86.67
5.250	.465	18.73	6.84	86.11
5.333	.468	18.87	6.84	86.67
5.500	.462	18.81	6.93	85.56
6.354	.451	18.67	7.07	83.52
6.500	.450	18.68	7.08	83.33
7.500	.451	18.64	7.06	83.52
7.833	.441	18.52	7.18	81.67
8.403	.431	18.40	7.32	79.81
8.875	.431	18.40	7.32	79.81
9.486	.431	18.42	7.32	79.81
10.708	.429	18.40	7.36	79.44
11.014	.424	18.34	7.42	78.52
11.521	.418	18.22	7.47	77.41
12.430	.416	18.22	7.52	77.04
12.587	.415	18.19	7.53	76.85
12.990	.413	18.17	7.54	76.48
13.420	.404	18.07	7.68	74.81
13.975	.409	18.12	7.60	75.74
	.411	19.48	8.12	
	.447	21.14	8.08	
	.470	22.42	8.08	

Table C-1--continued.

Aging Time t (days)	K_o	p' (psi)	q (psi)	K_o as % of Pre-Aging K_o
	.494	23.94	8.12	
	.513	24.98	8.04	
	.525	26.09	8.13	
	.535	27.06	8.20	
	.540	28.00	8.36	
	.538	29.48	8.85	

Table C-2 Test C: Values for σ_1', e, e in %, σ_3', and u

σ_1' (psi)	e	e as % of initial e	σ_3' (psi)	u (psi)
6.90	1.0501	83.86		
13.24	.9872	78.84		
25.63	.9197	73.45	14.27	32.98
25.64	.9181	73.32	13.70	32.97
25.68	.9176	73.28	13.03	32.93
25.70	.9175	73.27	13.12	32.91
25.69	.9172	73.25	13.11	32.92
25.70	.9168	73.22	12.61	32.91
25.73	.9165	73.19	12.38	32.88
25.76	.9164	73.18	12.12	32.85
25.71	.9163	73.18	12.03	32.90
25.73	.9163	73.18	12.04	32.88
25.57	.9161	73.16	11.89	33.04
25.71	.9161	73.16	12.03	32.90
25.74	.9161	73.16	11.88	32.87
25.74	.9159	73.14	11.60	32.87
25.75	.9158	73.14	11.60	32.86
25.70	.9156	73.12	11.58	32.91
25.69	.9156	73.12	11.34	32.92
25.72	.9155	73.11	11.08	32.89
25.72	.9153	73.10	11.08	32.89
25.75	.9153	73.10	11.10	32.86
25.76	.9152	73.09	11.05	32.85
25.76	.9150	73.09	10.92	32.85
25.69	.9150	73.07	10.75	32.92
25.73	.9149	73.07	10.70	32.88
25.71	.9148	73.06	10.66	32.90
25.71	.9148	73.06	10.63	32.89
25.74	.9148	73.06	10.39	32.87
25.72	.9147	73.05	10.51	32.89
27.60	.9132	72.93	11.35	32.95
29.21	.9114	72.78	13.06	32.95
30.49	.9092	72.61	14.34	32.97
32.06	.9059	72.35	15.83	32.96
33.01	.9026	72.08	16.94	32.97
34.22	.8989	71.79	17.96	33.01
35.25	.8971	71.64	18.86	33.24
36.36	.8943	71.42	19.63	33.43
38.33	.8807	70.33	20.63	33.02

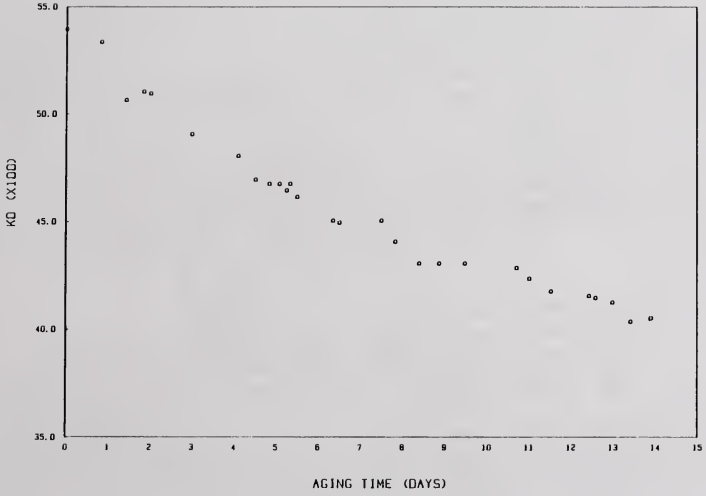

Figure C-1 Test C: K_o with Aging Time

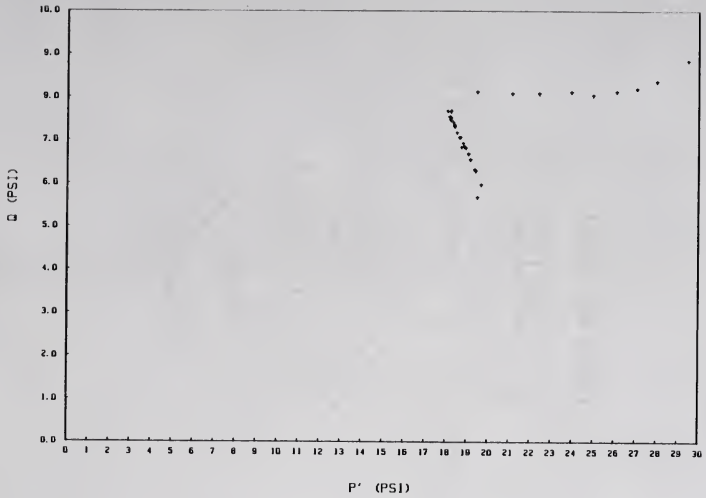

Figure C-2 Test C: p'-q Diagram

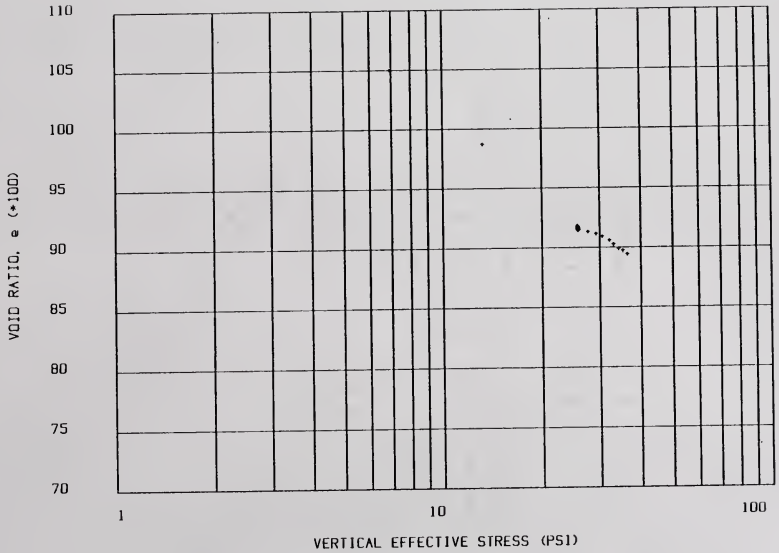

Figure C-3 Test C: e-log σ_1' Plot

APPENDIX D
TEST D: TABULATED RESULTS AND RAW PLOTS

Table D-1 Test D: Values for t, K_o, p', q, and K_o in %

Aging Time t (days)	K_o	p' (psi)	q (psi)	K_o as % of Pre-Aging K_o
0	.366	17.50	8.14	100
.0833	.360	17.44	8.20	98.36
.208	.346	17.27	8.40	94.54
.875	.313	16.89	8.83	85.52
1.208	.293	16.65	9.10	80.05
1.875	.278	16.49	9.32	75.96
3.625	.255	16.13	9.56	69.67
4.131	.260	16.21	9.52	71.04
4.333	.251	16.11	9.65	68.58
4.958	.252	16.14	9.65	68.85
5.541	.246	16.01	9.69	67.21
7.917	.244	16.05	9.75	66.67
8.132	.247	16.08	9.72	67.49
9.819	.228	15.84	9.96	62.30
10.361	.228	15.85	9.97	62.30
10.875	.221	15.77	10.07	60.38
12.257	.218	15.72	10.09	59.56
12.541	.218	15.73	10.11	59.56
13.125	.220	15.77	10.09	60.11
13.875	.214	15.63	10.13	58.47
14.375	.208	15.58	10.21	56.83
	.206	16.74	11.01	
	.206	16.74	11.01	
	.208	17.72	11.62	
	.218	18.66	11.98	
	.219	18.67	11.97	
	.221	19.65	12.55	
	.224	20.30	12.86	
	.227	21.11	13.29	
	.232	21.19	13.22	
	.229	21.90	13.74	

Table D-1--continued.

Aging Time τ (days)	K_o	p' (psi)	q (psi)	K_o as % of Pre-Aging K_o
	.233	21.99	13.67	
	.231	22.74	14.20	
	.236	22.84	14.11	
	.236	23.80	14.71	
	.241	24.83	15.19	

Table D-2 Test D: Values for σ_1', e, e in %, σ_3', and u

σ_1' (psi)	e	e as % of initial e	σ_3' (psi)	u (psi)
6.83	.7382	97.13		
13.20	.7279	95.78		
25.62	.7107	93.52	9.38	16.85
25.64	.7098	93.40	9.24	16.83
25.66	.7093	93.33	8.87	16.81
25.72	.7081	93.17	8.06	16.75
25.75	.7077	93.12	7.55	16.72
25.81	.7071	93.04	7.17	16.66
25.70	.7059	92.88	6.55	16.77
25.72	.7056	92.84	6.69	16.75
25.75	.7054	92.82	6.46	16.72
25.78	.7050	92.77	6.49	16.69
25.69	.7048	92.74	6.32	16.78
25.80	.7037	92.59	6.30	16.67
25.80	.7037	92.59	6.36	16.67
25.80	.7034	92.56	5.87	16.67
25.81	.7033	92.54	5.89	16.66
25.84	.7032	92.53	5.70	16.63
25.81	.7030	92.50	5.63	16.66
25.83	.7030	92.50	5.62	16.64
25.85	.7028	92.48	5.68	16.62
25.75	.7028	92.48	5.50	16.72
25.79	.7026	92.45	5.36	16.68
27.75	.7021	92.38	5.73	16.69
27.75	.7020	92.37	5.73	16.69
29.33	.7013	92.28	6.10	16.69
30.63	.7003	92.15	6.68	16.69
30.64	.7002	92.13	6.70	16.68
32.19	.6993	92.02	7.10	16.69
33.15	.6986	91.92	7.44	16.69
34.39	.6978	91.32	7.82	16.70
34.40	.6976	91.79	7.97	16.69
35.64	.6971	91.73	8.16	16.71
35.65	.6970	91.71	8.32	16.70
36.94	.6964	91.63	8.54	16.71
36.95	.6962	91.61	8.73	16.70
38.50	.6954	91.50	9.09	16.71
40.02	.6945	91.38	9.64	16.70

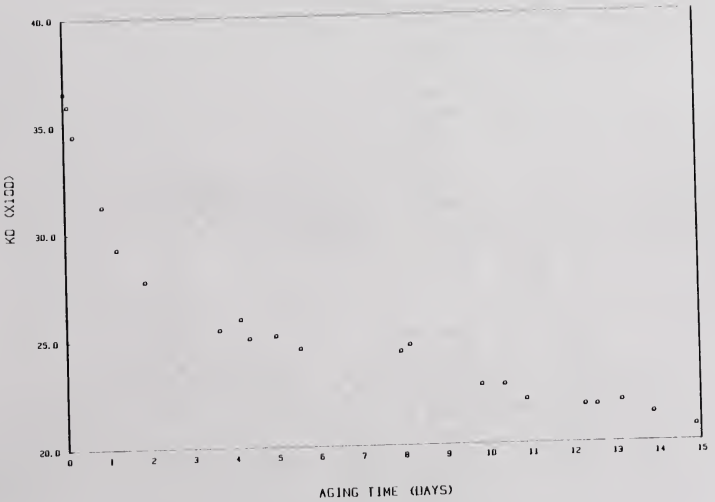

Figure D-1 Test D: K_o with Aging Time

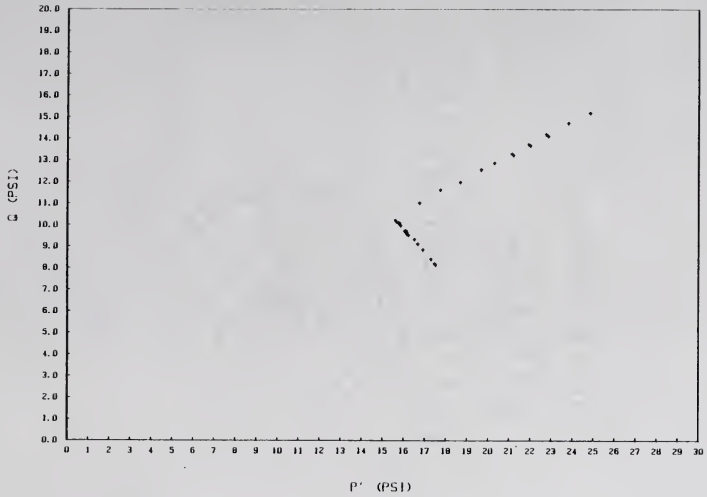

Figure D-2 Test D: p'-q Diagram

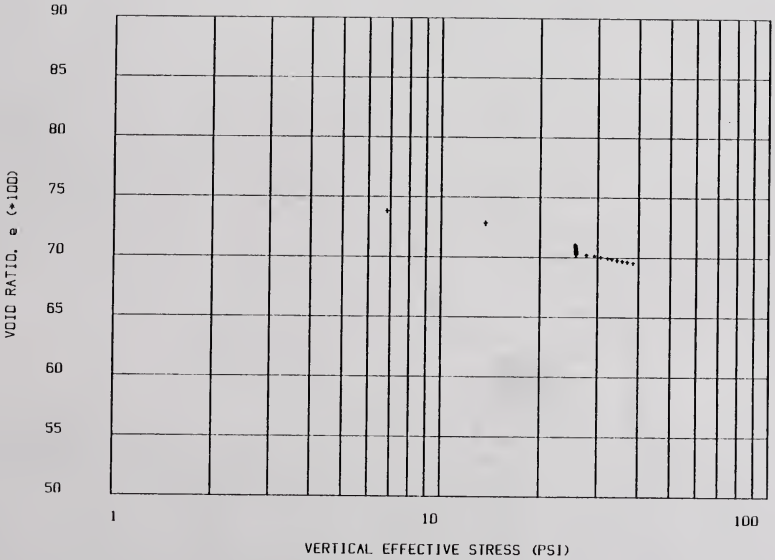

Figure D-3 Test D: e-log σ_1' Plot

APPENDIX E
TEST E: TABULATED RESULTS AND RAW PLOTS

Table E-1 Test E: Values for t, K_o, p', q, and K_o in %

Aging Time t (days)	K_o	p' (psi)	q (psi)	K_o as % of Pre-Aging K_o
0	.325	16.90	8.61	100
1.5	.268	16.25	9.39	82.46
2.806	.254	16.11	9.58	78.15
3.007	.255	16.11	9.57	78.46
4.000	.243	15.98	9.74	74.77
4.802	.239	15.94	9.80	73.54
5.000	.239	15.94	9.80	73.54
6.854	.244	16.06	9.76	75.08
9.208	.239	15.95	9.80	73.54
10.469	.236	15.94	9.84	72.62
11.180	.232	15.91	9.91	71.38
12.969	.228	15.89	9.99	70.15
13.260	.229	15.90	9.98	70.46
13.990	.222	15.84	10.07	68.31
	.212	16.88	10.98	
	.208	17.78	11.66	
	.210	18.57	12.12	
	.213	19.60	12.72	
	.214	20.20	13.08	
	.218	21.02	13.50	
	.217	21.78	14.00	
	.218	22.58	14.50	
	.217	23.50	15.14	
	.217	24.43	15.72	
	.218	25.40	16.30	

Table E-2 Test E: Values for σ_1', e, e in %, σ_3', and u

σ_1' (psi)	e	e as % of initial e	σ_3' (psi)	u (psi)
6.80	.7984	96.78		
13.14	.7868	95.37		
25.52	.7752	93.96	8.30	16.96
25.63	.7707	93.42	6.86	16.84
25.68	.7693	93.25	6.53	16.79
25.68	.7692	93.24	6.54	16.79
25.72	.7684	93.14	6.24	16.75
25.74	.7680	93.09	6.15	16.73
25.74	.7679	93.08	6.15	16.73
25.81	.7670	92.97	6.30	16.66
25.75	.7657	92.81	6.15	16.72
25.79	.7653	92.76	6.10	16.68
25.81	.7651	92.74	6.00	16.66
25.87	.7645	92.67	5.90	16.60
25.88	.7645	92.67	5.92	16.59
25.91	.7642	92.63	5.77	16.56
27.87	.7641	92.62	5.90	16.57
29.43	.7638	92.58	6.12	16.59
30.69	.7636	92.56	6.45	16.63
32.31	.7631	92.50	6.88	16.57
33.27	.7627	92.45	7.12	16.57
34.52	.7623	92.40	7.51	16.57
35.78	.7618	92.34	7.77	16.57
37.08	.7613	92.28	8.07	16.57
38.64	.7607	92.21	8.37	16.57
40.15	.7601	92.13	8.71	16.57
41.70	.7594	92.05	9.11	16.57

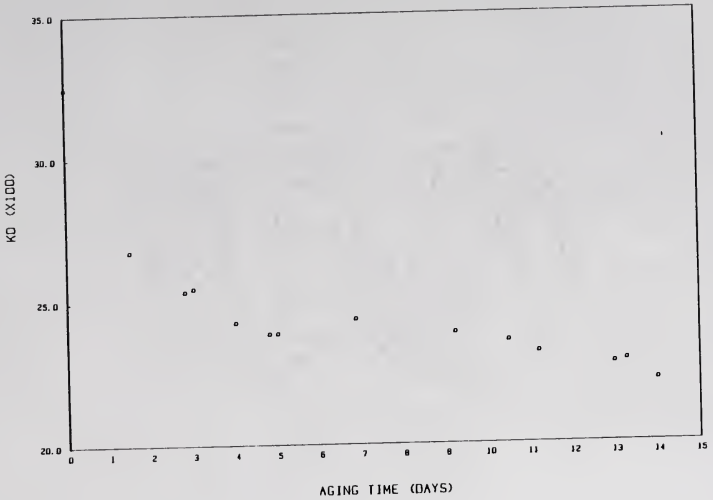

Figure E-1 Test E: K_o with Aging Time

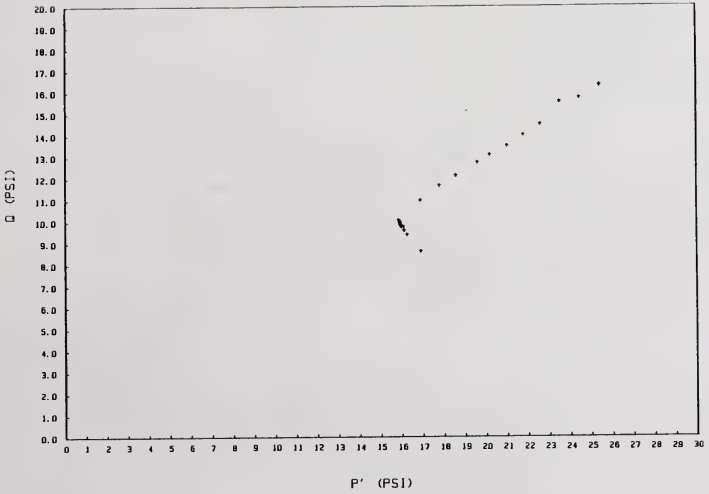

Figure E-2 Test E: p'-q Diagram

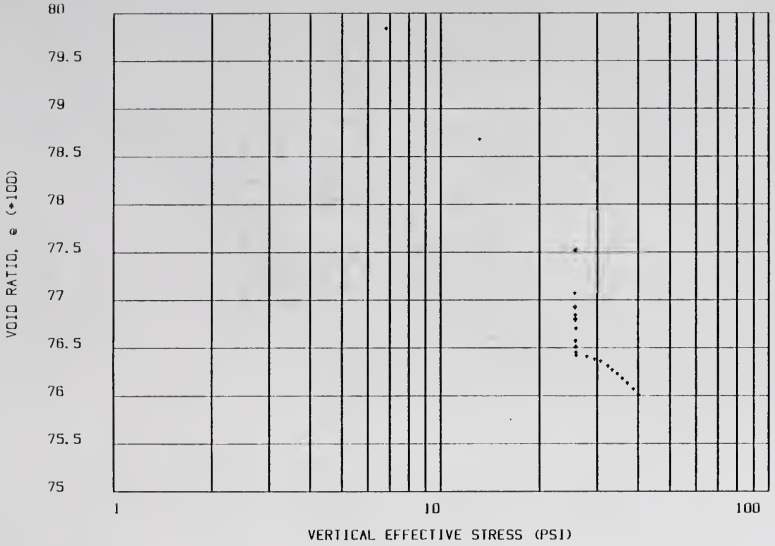

Figure E-3 Test E: e-log σ_1' Plot

APPENDIX F
TEST F: TABULATED RESULTS AND RAW PLOTS

Table F-1 Test F: Values for t, K_o, p', q, and K_o in %

Aging Time t (days)	K_o	p' (psi)	q (psi)	K_o as % of Pre-Aging K_o
0	.632	21.70	3.83	100
.8125	.626	20.75	4.78	99.05
1.062	.611	20.58	4.96	96.68
1.760	.586	20.25	5.28	92.72
1.823	.587	20.26	5.28	92.88
2.250	.565	20.00	5.56	89.40
2.740	.565	19.99	5.56	89.40
3.200	.555	19.87	5.69	87.82
3.462	.555	19.89	5.69	87.82
4.042	.531	19.58	5.99	84.02
4.326	.531	19.58	6.00	84.02
4.750	.525	19.50	6.08	83.07
5.086	.518	19.43	6.17	81.96
5.660	.499	19.20	6.41	78.96
6.323	.492	19.10	6.50	77.85
6.740	.492	19.11	6.51	77.85
7.705	.460	18.72	6.92	72.78
7.833	.463	18.74	6.88	73.26
8.406	.456	18.65	6.97	72.15
9.125	.457	18.69	6.97	72.31
9.250	.453	18.63	7.01	71.68
10.132	.438	18.45	7.22	69.30
11.323	.425	18.27	7.38	67.25
11.740	.419	18.23	7.46	66.30
12.010	.419	18.23	7.47	66.30
12.677	.409	18.12	7.60	64.72
13.573	.397	17.94	7.74	62.82
	.449	20.02	7.61	
	.442	19.92	7.71	
	.468	21.45	7.77	
	.504	22.93	7.57	

Table F-1--continued.

Aging Time t (days)	K_o	p' (psi)	q (psi)	K_o as % of Pre-Aging K_o
	.535	24.60	7.46	
	.564	25.81	7.20	
	.579	27.05	7.21	
	.601	28.43	7.08	
	.610	29.63	7.17	
	.610	29.63	7.17	
	.624	31.16	7.21	
	.624	31.17	7.21	
	.632	32.54	7.34	
	.632	32.54	7.34	

Table F-2 Test F: Values for σ_1', e, e in %, σ_3', and u

σ_1' (psi)	e	e as % of initial e	σ_3' (psi)	u (psi)
6.78	.7328	89.74		
13.12	.7152	87.58		
25.52	.6918	84.72	16.13	16.95
25.53	.6906	84.57	15.97	16.74
25.54	.6904	84.54	15.61	16.93
25.53	.6900	84.49	14.97	16.94
25.54	.6899	84.48	14.98	16.93
25.55	.6896	84.44	14.44	16.92
25.55	.6893	84.41	14.43	16.92
25.55	.6890	84.37	14.18	16.92
25.57	.6890	84.37	14.20	16.90
25.57	.6885	84.31	13.59	16.90
25.57	.6884	84.30	13.58	16.90
25.57	.6883	84.29	13.42	16.90
25.60	.6881	84.26	13.26	16.87
25.61	.6879	84.24	12.79	16.86
25.60	.6876	84.20	12.60	16.87
25.61	.6874	84.18	12.60	16.86
25.63	.6872	84.15	11.80	16.84
25.62	.6871	84.14	11.86	16.85
25.62	.6869	84.12	11.68	16.85
25.65	.6867	84.09	11.72	16.82
25.64	.6866	84.08	11.62	16.83
25.66	.6863	84.04	11.23	16.81
25.65	.6860	84.00	10.89	16.82
25.69	.6860	84.00	10.77	16.78
25.69	.6856	83.96	10.76	16.78
25.72	.6853	83.92	10.52	16.75
25.67	.6851	83.89	10.20	16.80
27.63	.6840	83.76	12.41	16.81
27.63	.6840	83.76	12.21	16.81
29.21	.6828	83.61	13.68	16.81
30.49	.6813	83.43	15.36	16.83
32.05	.6798	83.24	17.14	16.83
33.01	.6784	83.07	18.61	16.83
34.25	.6770	82.90	19.84	16.84
35.51	.6757	82.74	21.35	16.84
36.80	.6745	82.60	22.46	16.85
36.80	.6744	82.58	22.46	16.85

Table F-2--continued.

σ_1' (psi)	e	e as % of initial e	σ_3' (psi)	u (psi)
38.36	.6730	82.41	23.95	16.85
38.37	.6728	82.39	23.96	16.84
39.87	.6718	82.27	25.20	16.85
39.88	.6713	82.20	25.20	16.84

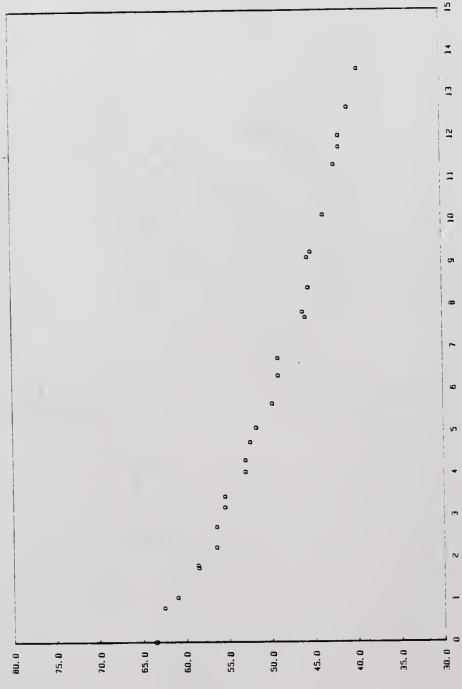

Figure F-1 Test F: K_o with Aging Time

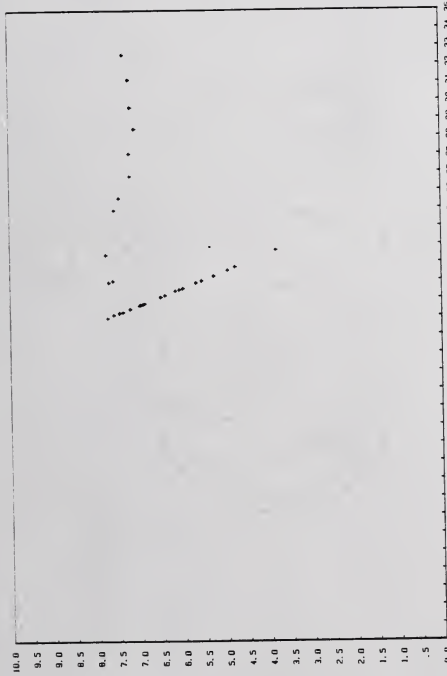

Figure F-2 Test F: p'-q Diagram

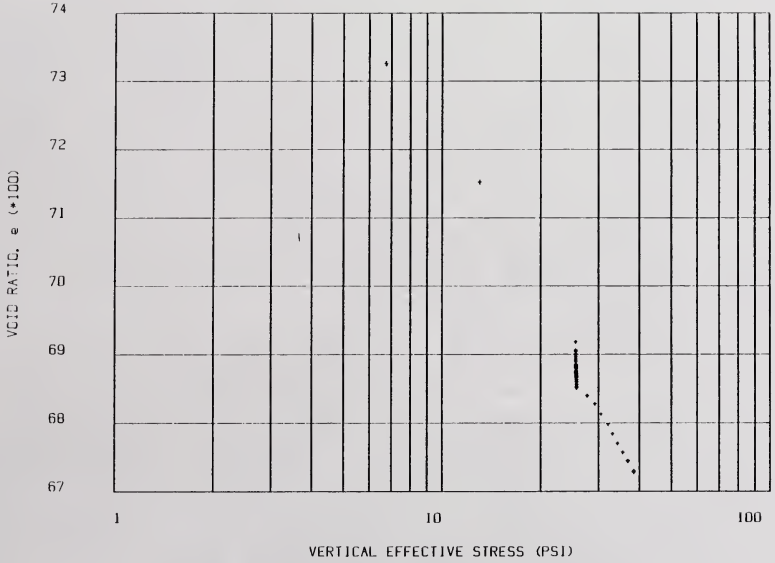

Figure F-3 Test F: e-log σ_1' Plot

APPENDIX G
EPKW AND NOVW: RESULTS OF CONVENTIONAL OEDOMETER TESTS

Table G-1 EPKW and NOVW: Conventional Oedometer Test Specimen Data

	Units	Soil →	EPKW	NOVW
w	%		40.43	20.97
W	g		138.11	140.80
d	cm		6.288	6.276
	in		2.476	2.471
H	cm		2.587	2.556
	in		1.018	1.006
G_s			2.59	2.65
A	cm^2		31.054	30.903
	in^2		4.815	4.796
V	cc		80.329	79.056
	in^3		4.902	4.824
V_s	cc		37.972	43.921
	in^3		2.317	2.680
H_s	cm		1.222	1.420
	in		0.481	0.559
e_o			1.1157	0.8000
γ	g/cc		1.719	1.781

Table G-2 EPKW and NOVW: Values for σ_1', e, and e in % for Conventional Oedometer Tests

Soil	σ_1' (psi)	e	e as % of initial e
EPKW	3.47	1.0600	95.01
	6.94	1.0263	91.99
	13.89	0.9813	87.95
	27.78	0.9324	83.57
	55.56	0.8769	78.60
	111.11	0.8172	73.24
NOVW	3.47	0.7943	99.29
	6.94	0.7897	98.71
	13.89	0.7794	97.43
	27.78	0.7735	96.69
	55.56	0.7653	95.66
	111.11	0.7555	94.44

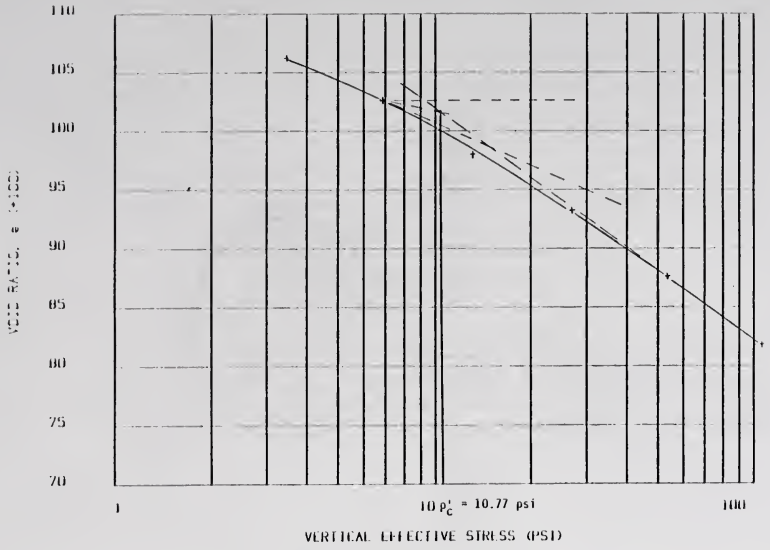

Figure G-1 EPKW: e-log σ_1' Plot for Conventional Oedometer Test

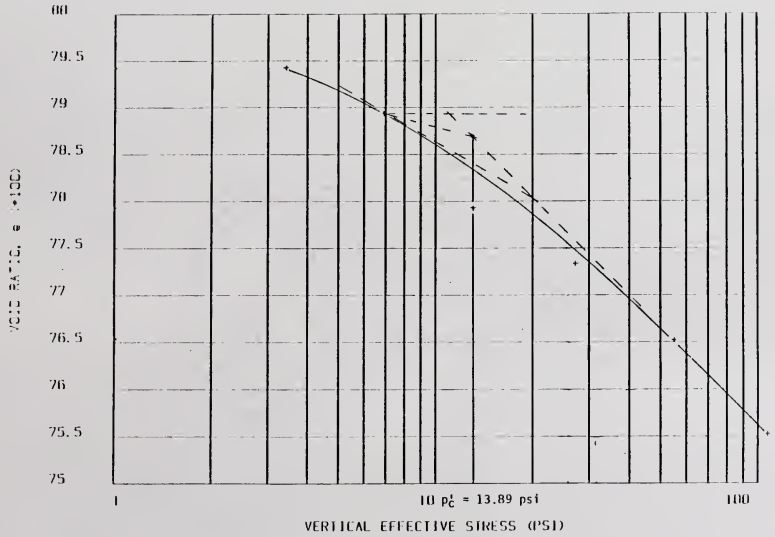

Figure G-2 NOVW: e-log σ_1' Plot for Conventional Oedometer Test

APPENDIX H
SAMPLE q-p_c EFFECT CALCULATIONS

This appendix provides a step-by-step guide for calculating the information in Table 5-4. Calculations shown are for Test A.

(1) Normal Consolidation Pressure, $p_o = \sigma_1'$

$p_o = \sigma_1' = \sigma_1 - u = 86.31 - 60.68 = 25.63$ psi;

σ_1 = total vertical stress known from oedometer calibration;

u = backpressure reading before placement of final load since excess pore water pressure from previous load has dissipated.

(2) Slope of Initial K_o-Line, S_2

$S_2 = (1-K_o \text{ @ point 2})/(1+K_o \text{ @ point 2}) = (1-.457)/(1+.457)$
$= .373$

(3) Slope of K_o-Line After q-p_c Effect, S_4

$S_4 = (1-K_o \text{ @ point 4})/(1+K_o \text{ @ point 4}) = (1-.282)/(1+.282)$
$= .560$

(4) Net Effect of A over the entire 2-4 ESP of the q-p_c Process, A_q

$$A_q = \frac{p_2'-p_4'+q_4-q_2}{2(q_4-q_2)} = \frac{18.76 - 18.20 + 10.20 - 7.00}{2(10.20 - 7.00)} = .588$$

(5) Magnitude of q-p_c Effect from Schmertmann's Theory, Δp_{cq}

$$\Delta p_{cq} = p_o \frac{2(1-A_q)(S_4-S_2)}{[1-(1-2A_q)S_4](1+S_2)} = 25.63 \frac{2(1-.588)(.560-.373)}{[1-\{1-2(.588)\}.560](1+.373)}$$

$= 2.52$ psi

(6) Magnitude of q-p_c Effect from e-log σ_1' Plot, Δp_{cq}

Δp_{cq} = (σ_1' at the end of the q-p_c effect)-(p_o=σ_1')

= 32.42 - 25.63 = 6.79 psi

The end of the q-p_c effect is defined as the first departure from a straight line through the small load void ratios. The numerical value for σ_1' is determined by interpolating between points with known σ_1' values.

σ_1' at the end of the q-p_c effect = 31.26 + .8(32.71 - 31.26)

= 32.42 psi

(7) Predicted Increase in Load Capacity Due to q-p_c Effect, $\Delta p_{cq\ theory}/p_o$

$$\% \text{ Increase} = \frac{\Delta p_{cq\ theory}}{p_o} * 100 = \frac{2.62 \text{ psi}}{25.63 \text{ psi}} * 100 = 10.22\%$$

(8) Graphically-Determined Increase in Load Capacity Due to q-p_c Effect, $\Delta p_{cq\ plot}/p_o$

$$\% \text{ Increase} = \frac{\Delta p_{cq\ plot}}{p_o} * 100 = \frac{6.79 \text{ psi}}{25.63 \text{ psi}} * 100 = 26.49\%$$

(9) Quantitative Theory Prediction vs. Graphical Solution

Difference = % Increase (Theory) - % Increase (Graphical)

= 10.22 - 26.49 = 16.27%

BIBLIOGRAPHY

Allam, Mehter M., and A. Sridharan, Discussion of "A Simple Question About Consolidation," Journal of Geotechnical Engineering, American Society of Civil Engineers, Vol. 110, No. 5, May, 1984, pp. 671-672.

Bjerrum, Laurits, "Engineering Geology of Norwegian Normally-Consolidated Marine Clays as Related to Settlements of Buildings," Geotechnique, The Institution of Civil Engineers, Vol. 17, No. 2, June, 1967, pp. 81-118.

Bjerrum, Laurits, "Embankments on Soft Ground," Proceedings of the Specialty Conference on Performance of Earth and Earth-Supported Structures, American Society of Civil Engineers, Vol. 2, June, 1972, pp. 1-55.

Bjerrum, Laurits, and T.H. Wu, "Fundamental Shear Strength Properties of the Lilla Edet Clay," Geotechnique, The Institution of Civil Engineers, Vol. 10, No. 3, September, 1960, pp. 101-109.

Borja, Ronaldo I., Finite Element Analysis of the Time-Dependent Behavior of Soft Clays, Ph.D. Dissertation, Civil Engineering Department, Stanford University, Stanford, California, April, 1984.

Casagrande, Arthur, "The Determination of the Pre-Consolidation Load and Its Practical Significance," Proceedings of the First International Conference on Soil Mechanics and Foundation Engineering, Vol. 1, 1936, pp. 60-64.

Davidson, John L., The Effect of Quasi-Preconsolidation on Compression of Clay Soils, Ph.D. Dissertation, Civil Engineering Department, Purdue University, Lafayette, Indiana, August, 1973.

Davidson, John L., "A Quasi-Preconsolidation Clay Model," Proceedings of the Ninth International Conference on Soil Mechanics and Foundation Engineering, Vol. 1, 1977, pp. 75-79.

Hanzawa, Hideo, "Undrained Strength Characteristics of Normally Consolidated Aged Clay," Soils and Foundations, The Japanese Society of Soil Mechanics and Foundation Engineering, Vol. 23, No. 3, September, 1983, pp. 39-49.

Hsieh, Hsii-Sheng, An Automated Triaxial Device for Measuring the At-Rest Earth Pressure Coefficient, Engineer's Thesis, Civil Engineering Department, Stanford University, Stanford, California, August, 1984.

Jamiolkowski, M., C.C. Ladd, J.T. Germaine, and R. Lancellotta, "New Developments in Field and Laboratory Testing of Soils," Pre-Print of State-of-the-Art Paper for Eleventh International Conference on Soil Mechanics and Foundation Engineering, 1985, pp. 30-33.

Kavazanjian, Edward, Jr., and James K. Mitchell, "Time Dependence of Lateral Earth Pressure," Journal of Geotechnical Engineering, American Society of Civil Engineers, Vol. 110, No. 4, April, 1984, pp. 530-533.

Lambe, T. William, "A Mechanistic Picture of Shear Strength in Clay," Proceedings of the ASCE Research Conference on Shear Strength of Cohesive Soils, American Society of Civil Engineers, 1960, pp. 555-580.

Leonards, G.A., and A.G. Altschaeffl, "Compressibility of Clay," Journal of the Soil Mechanics and Foundations Division, American Society of Civil Engineers, Vol. 90, No. SM5, September, 1964, pp. 133-155.

Manzione, Charles W., Construction and Operation of the University of Florida K_o-Consolidometer, Master of Engineering Report, Civil Engineering Department, University of Florida, Gainesville, Florida, August, 1985.

McRoberts, Ed, Discussion of "A Simple Question About Consolidation," Journal of Geotechnical Engineering, American Society of Civil Engineers, Vol. 110, No. 5, May, 1984, pp. 667-669.

Nagaraj, T.S., Discussion of "A Simple Question About Consolidation," Journal of Geotechnical Engineering, American Society of Civil Engineers, Vol. 110, No. 5, May, 1984, pp. 665-667.

Schmertmann, John H., "A General Time-Related Soil Friction Increase Phenomenon," Laboratory Shear Strength of Soil, ASTM STP 740, R.N. Yong and F.C. Townsend, Eds., American Society for Testing and Materials, Philadelphia, Pennsylvania, 1981, pp. 456-484.

Schmertmann, John H., "A Simple Question About Consolidation," Journal of Geotechnical Engineering, American Society of Civil Engineers, Vol. 109, No. 1, January, 1983, pp. 119-122.

Schmertmann, John H., Closure of "A Simple Question About Consolidation," Journal of Geotechnical Engineering, American Society of Civil Engineers, Vol. 110, No. 5, May, 1984, p. 673.

Soydemir, Cetin, Discussion of "A Simple Question About Consolidation," Journal of Geotechnical Engineering, American Society of Civil Engineers, Vol. 110, No. 5, May, 1984, pp. 669-671.

Stoutamire, W.D., The Design and Construction of a K_o-Consolidometer to Measure Lateral Stresses, Engineer's Thesis, Civil Engineering Department, University of Florida, Gainesville, Florida, December, 1982.

Tan, Tjong-Kie, "Structure Mechanics of Clays," Academia Sinica, Institute of Civil Engineering and Architecture-Harbin (China), June, 1957.

Terzaghi, Karl, "Undisturbed Clay Samples and Undisturbed Clays," Journal, Boston Society of Civil Engineers, Vol. 28, No. 3, July, 1941, pp. 211-231.

Yasuhara, Kazuya, "Secondary Compression of Soft Clay in Consolidation and Shear Tests," Proceedings of Symposium on Recent Development in Laboratory and Field Tests and Analysis in Geotechnical Problems, Asian Institute of Technology, 1983, pp. 1-7.

Yasuhara, Kazuya, "Does K_o Change During Secondary Compression?," Pre-Print for Annual Meeting of Kyushu Branch of JSCE, Part III, 1984.

Yasuhara, Kazuya, and Syunji Ue, Closure of "Increase in Undrained Strength Due to Secondary Compression," Soils and Foundations, The Japanese Society of Soil Mechanics and Foundation Engineering, Vol. 24, No. 3, September, 1984, pp. 115-119.

BIOGRAPHICAL SKETCH

Randall Wayne Brown was born June 15, 1956, in Blakely, Georgia. His family moved to Dothan, Alabama, in 1957. He attended public schools in Dothan and graduated from Dothan High School in 1974. He entered Auburn University in 1974 and became active in several organizations including Chi Epsilon, Scabbard and Blade, Air Force ROTC, and the student chapter of the American Society of Civil Engineers (ASCE), serving the latter as President during his senior year. He graduated in June 1978 with the Bachelor of Civil Engineering degree, an Air Force commission, and the Distinguished Military Graduate designation.

While awaiting his first active duty assignment, he worked for the City Engineer in Dothan. In September 1978, he moved to Kirtland AFB in Albuquerque, New Mexico, to begin a three-year tour as a geotechnical engineer at the Air Force Weapons Laboratory (AFWL). While at AFWL, he was involved primarily with soil dynamics problems associated with the design and basing of the MX-missile.

In August 1981, Brown moved to Gainesville to attend the University of Florida under the Air Force Institute of Technology Civilian Institution (AFIT/CI) Program. He received the Master of Engineering degree with a concentration in construction engineering

in December 1982. He entered the doctoral specialization in geotechnical engineering in January 1983.

Brown is an Associate Member of ASCE and recently completed a term on the Aerospace Division Awards and Publications Committee. Professional registration is the next goal in Brown's engineering career.

Captain Brown is married to the former Brenda Jean Watford of Dothan. They have a 21-month old son, Matthew. The Browns are active in Highland Missionary Baptist Church in Gainesville. They enjoy sports and travel.

I certify that I have read this study and that in my opinion it conforms to acceptable standards of scholarly presentation and is fully adequate, in scope and quality, as a dissertation for the degree of Doctor of Philosophy.

John L. Davidson, Chairman
Associate Professor of Civil Engineering

I certify that I have read this study and that in my opinion it conforms to acceptable standards of scholarly presentation and is fully adequate, in scope and quality, as a dissertation for the degree of Doctor of Philosophy.

James H. Schaub
Professor of Civil Engineering

I certify that I have read this study and that in my opinion it conforms to acceptable standards of scholarly presentation and is fully adequate, in scope and quality, as a dissertation for the degree of Doctor of Philosophy.

Frank C. Townsend
Professor of Civil Engineering

I certify that I have read this study and that in my opinion it conforms to acceptable standards of scholarly presentation and is fully adequate, in scope and quality, as a dissertation for the degree of Doctor of Philosophy.

Kermit L. Hall
Professor of History

This dissertation was submitted to the Graduate Faculty of the College of Engineering and to the Graduate School, and was accepted as partial fulfillment of the requirements for the degree of Doctor of Philosophy.

August 1985

Hubert A. Bowers
Dean, College of Engineering

Dean, Graduate School